Norwegian University of Life Sciences

Master's Thesis 2018 30 ECTS
Faculty of Science and Technology
Supervisor: Espen Olsen

Temperature- and irradiation-dependent properties of photochromic thin films of YH_x:O

Ragnhild Svellingen Hallaråker
Environmental Physics and Renewable Energy
Faculty of Science and Technology

Preface

This project was initiated by the Solar Department at the Institute for Energy Technology (IFE), as a conclusion to my M. Sc. degree in Environmental Physics and Renewable Energy. Project funding was granted through the Norwegian Research Council's FRINATEK program. The work was carried out at IFE's research facilities, which is the centre of expertise for the material in question.

Writing this thesis turned out to be a quandary on more levels than I could ever have foreseen. The topic in general has made me increasingly aware that I currently have one foot in the field of materials' physics, and the other in the field of applied engineering. The result is an attempt to mix the best of both worlds, in the hope that it will be of some benefit to the scientific community. Behind the scenes, I have also been fortunate enough to get a sneak peek of the business-related aspects of innovative science. The psychological assessment of writing a master's thesis would likely be able to fill a chapter of its own as well.

I am truly grateful to everyone who's supported me through this process. A big "thank you" to my supervisors is highly called for, for all their interest, patience and backing-up. In random order: Thank you, José Montero and Fredrik Martinsen, for teaching me how to have fun in a lab full of scary, expensive equipment. Thank you, Smagul Karazhanov, for sharing your knowledge and enthusiasm about the strange world of materials' physics. Thank you, Erik Marstein and Espen Olsen, for making sure that my hopelessly chaotic ideas made their way into a structured thesis. Thank you to the research community at IFE, for including me in your team and showing me that being a science geek can indeed be both fun and socially rewarding. Last, but not least: Thank you to my mum and boyfriend, for ensuring a steady supply of coffee and chocolate.

I would like to dedicate this thesis to my dad, the scientist-in-disguise whom I know would have taken great joy in reading (parts of) it.

Kjeller, 07.05.2018

Ragnhild Svellingen Hallaråker

Abstract

Oxygen-containing yttrium hydride (YH_x:O) thin films exhibit photochromic behaviour, in which transparent films reversibly darken upon illumination by visible and ultraviolet radiation. This feature has motivated intense research, due to its potential application in ophthalmic lenses and smart windows. The commercialization of such applications requires a thorough understanding of the underlying reaction mechanisms, as well as how these are affected by ambient conditions.

Through the work presented in this thesis, a reliable method was developed for the investigation of temperature- and irradiation-dependent changes in the photochromic effect of YH_x:O. The investigations revealed that photodarkening and bleaching characteristics strongly depends on temperature and incident radiation intensity. While increasing the temperature will decrease the photodarkening rate and increase the bleaching rate, the opposite was observed when increasing the incident intensity. The results were quantified by the calculation of time constants, equilibrium transmittances and the activation energy. A possible explanation to the observed results was suggested by the classification of YH_x:O as a photothermochromic material, in which transmission changes are driven by photoinduced electronic transitions and thermally induced atomic rearrangements.

Sammendrag

Oksygenholdige tynnfilmer av yttriumhydrid (YH_x:O) er et fotokromatisk materiale, som undergår en reversibel formørkning når det bestråles med synlig og ultrafiolett lys. Mulige bruksområder som solbriller og smarte vinduer har motivert omfattende forskning de siste årene. Kommersialiseringen av slike produkter forutsetter en grundig forståelse av de bakenforliggende reaksjonsmekanismene, og hvordan disse påvirkes av omgivelsene.

Formålet med denne oppgaven var blant annet å utvikle en pålitelig metode for studiet av temperatur- og innstrålingsavhengige endringer i den fotokromatiske effekten i YH_x:O. Undersøkelsene viste at viktige egenskaper ved transmisjonsendringene er avhengige av temperatur og innstrålingsintensitet. En økning i temperaturen reduserte formørknings-hastigheten og økte blekehastigheten merkbart, mens det motsatte ble observert ved en økning av innstrålingsintensitet. Resultatene ble kvantifisert ved beregning av tidskonstanter, likevektstransmittanser og aktiveringsenergi. Klassifiseringen av YH_x:O som et fototermokromatisk materiale ble foreslått som en mulig forklaring på de observerte resultatene. Denne modellen innebærer at transmisjonsendringene drives av lysinduserte elektronoverganger og termisk induserte omorganiseringer av YH_x:O-molekylene.

Contents

Preface I

Sammendrag (Norwegian abstract) II

Abstract III

1 Introduction 1

2 Theory 3

2.1 Chromism . . . 3

2.2 Photochromism . . . 7

2.3 Oxygen-containing yttrium hydrides . . . 13

3 Methods 17

3.1 Synthesis . . . 17

3.2 Optical measurements . . . 19

3.3 Analysis . . . 24

4 Results and discussion 26

4.1 Initial sample properties . . . 26

4.2 Photochromism at standard laboratory conditions . . . 28

4.3 The effect of temperature . . . 29

4.4 The effect of intensity . . . 37

4.5 The effect of wavelength . . . 41

4.6 Reaction mechanisms . . . 43

5 Conclusions and further work 46

References 47

Appendix 52

A1. Initial sample properties . . . 53

A2. Filter properties . . . 55

A3. The effect of temperature. . . . 57

A4. The effect of wavelength. . . . 59

1. Introduction

The problems related to our ever-increasing energy consumption, such as climate change and energy shortages, have been the cause of great concerns for several decades. Nevertheless, global energy demands are expected to continue to increase considerably, as a result of population growth, improved living standards, urbanization – and climate change itself. Currently, the building sector accounts for about 30 % of global energy consumption, much of which is attributed to inefficient windows[1]. Windows typically transmit either too much or too little energy, contributing to the need for artificial cooling and heating. According to the IEA, reducing cooling/heating demands in hot/cold climates could bring about energy savings corresponding to 10-40 % / 20-30 % of average building energy requirements, respectively[2]. Consequently, the importance of developing more energy-efficient windows is both evident and urgent.

One of several necessary solutions to this challenge may be the so-called *smart windows.* Similar to the solar control and low-emissivity glazing already applied in a lot of windows, smart windows regulate the transmission of either solar or thermal radiation through the window. In contrast to static glazing, however, smart windows are also able to respond to fluctuations in ambient conditions and users' needs. This enables great energy savings of up to >20 %[3].

The material investigated in this project – oxygen-containing yttrium hydride (YH_x:O) – was discovered as a possible smart window candidate in 2011. When illuminated by visible and ultraviolet light, the transmissivity of YH_x:O is reduced by up to 50 %. Subsequently, it will regenerate to its initial yellowish colour when left in the dark. This made it the first rare-earth metal hydride known to experience *photochromism* – a reversible colour-change upon illumination. Photodarkening of YH_x:O is demonstrated in *Figure 1.1* by Trygve Mongstad, who also discovered the phenomenon.

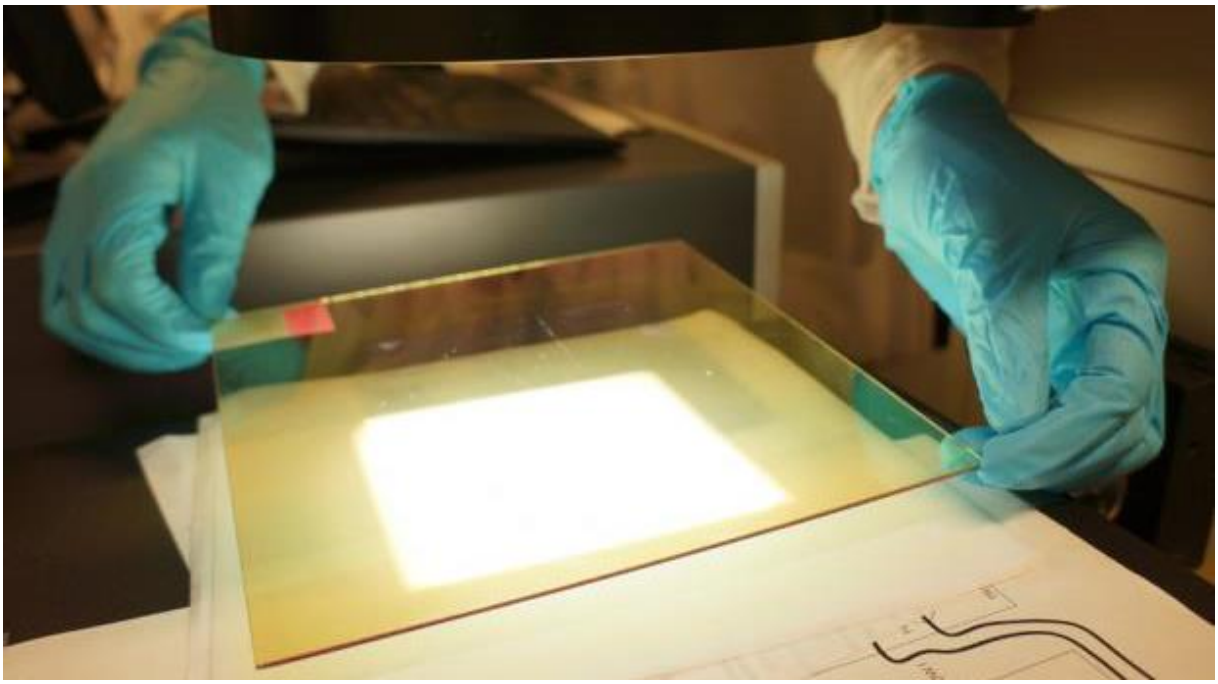

Figure 1.1: Photochromic YH_x:O being illuminated with a solar simulator, resulting in a visible darkening of the thin-film. The picture is taken at the Department for Solar Energy at the Institute for Energy Technology (IFE). (Photo: Arnfinn Christensen)

Thin films of YH_x:O are considered suitable not only for smart window coatings: they are also relevant to certain space applications, automotive sunroofs and contrast-enhancing photochromic glasses. The latter have already proved popular in the commercial market, using materials other than YH_x:O. What makes YH_x:O superior to competing photochromic materials (e.g. WO_3), is its colour-neutral photodarkening across the entire visible and infrared spectrum. Furthermore, recent discoveries of vast yttrium deposits are likely to reduce future costs, as yttrium is no longer considered "rare"[4].

Since its discovery, a lot of effort has been put into unravelling the reaction mechanisms of YH_x:O. A complete comprehension would open the doors to possible tuning of the material properties, as well as the discovery of similar photochromic materials. The existing theories include electronic excitations, molecular rearrangements and the formation of dark metallic domains. However, some of the observations made so far seem contradictory, and thus the result currently remains inconclusive.

The commercialization of YH_x:O also relies on the knowledge of how the material behaves at different ambient conditions. Factors such as the time- and location dependence of transmission changes, as well as the corresponding reaction rates greatly determines what can be considered promising applications. Moreover, the same parameters may give important clues regarding the reaction mechanisms. So far, only a few preliminary and qualitative observations have been made regarding light intensity and sample temperature.

The objective of this thesis is to establish a proper, quantitative understanding of the main effects of ambient conditions on the photochromism of YH_x:O. Important photochromic parameters, such as reaction kinetics and changes in transmission, will be monitored at different temperatures, incident intensities and wavelengths, by the use of optical techniques. Because controlled heating of YH_x:O has never been attempted before, part of the goal is to deduce an appropriate way of doing so. The repeatability of the experiments is also investigated, as this will provide important information regarding the reliability of both the material and experimental procedures. The results will be related to the possibilities and limitations of future applications, and – if possible – to the underlying reaction mechanisms.

2. Theory

2.1 – Chromism

Chromism is defined as a process involving *a reversible colour change in a substance, induced by some external stimulus*. Depending on their applications, the materials that exhibit this property are termed either *chromic* or *chromogenic*. Owing to their wide range of existing and possible applications, chromogenics have been the subject of intense research for several decades. This section will focus on the relevance of chromogenic materials in modern window technologies.

2.1.1 – Radiation control

Present-day windows are expected to fulfil a vast number of requirements. Although their primary purposes are still indoor-outdoor contact and daytime illumination, modern windows should also provide functions such as environmental protection, thermal insulation, safety/security enhancement, ventilation, decoration and incoming/outgoing radiation control. The material investigated in this project is dedicated to the latter of these concerns.

Simply put, the objective of radiation control is to filter out unwanted parts of the available radiation, while utilizing parts that are beneficial to the specific application. Generally, the distinction between wanted and unwanted radiation is based on its wavelength and angle of incidence, leading to so-called *angularly selective* and *spectrally selective* windows. Angularly selective windows will most often transmit normally incident radiation (which is needed in visual indoor-outdoor contact), and discard high-angle midday solar rays (which could otherwise cause glare and overheating). Spectrally selective windows will typically tune the amount of thermal radiation allowed into/out of the window according to heating/cooling requirements, while still admitting visible light.

Figure 2.1 (next page) introduces the foundations for spectral selectivity, showing the wavelength-dependent spectra of *(a)*: black-body radiation at four different temperatures, *(b)*: extra-terrestrial solar radiation, *(c)*: atmospheric absorptance at sea level, and *(d)*: the radiation useful to photosynthesis/greenhouses and the human eye[5]. As *Figure 2.1* illustrates, there is almost no overlap between the thermal radiation spectrum *(a)* and the solar spectrum *(b)*. This important observation is famously described by Wien's displacement law, stating that the emission peaks are displaced towards shorter wavelengths as the temperature of the radiating object increases. As a result, it is possible to obtain windows that interact differently with the different spectra. When considering the atmospheric absorptance depicted in *(c)*, it is evident that most of the solar radiation is transmitted to ground level – including visible light *(d*). Because the radiation useful for human vision is limited to the wavelength range of $0.4 < \lambda < 0.7\ \mu m$, the remaining ~50 % of the irradiated solar energy (mainly in the infrared domain) may often be discarded or utilized otherwise[5].

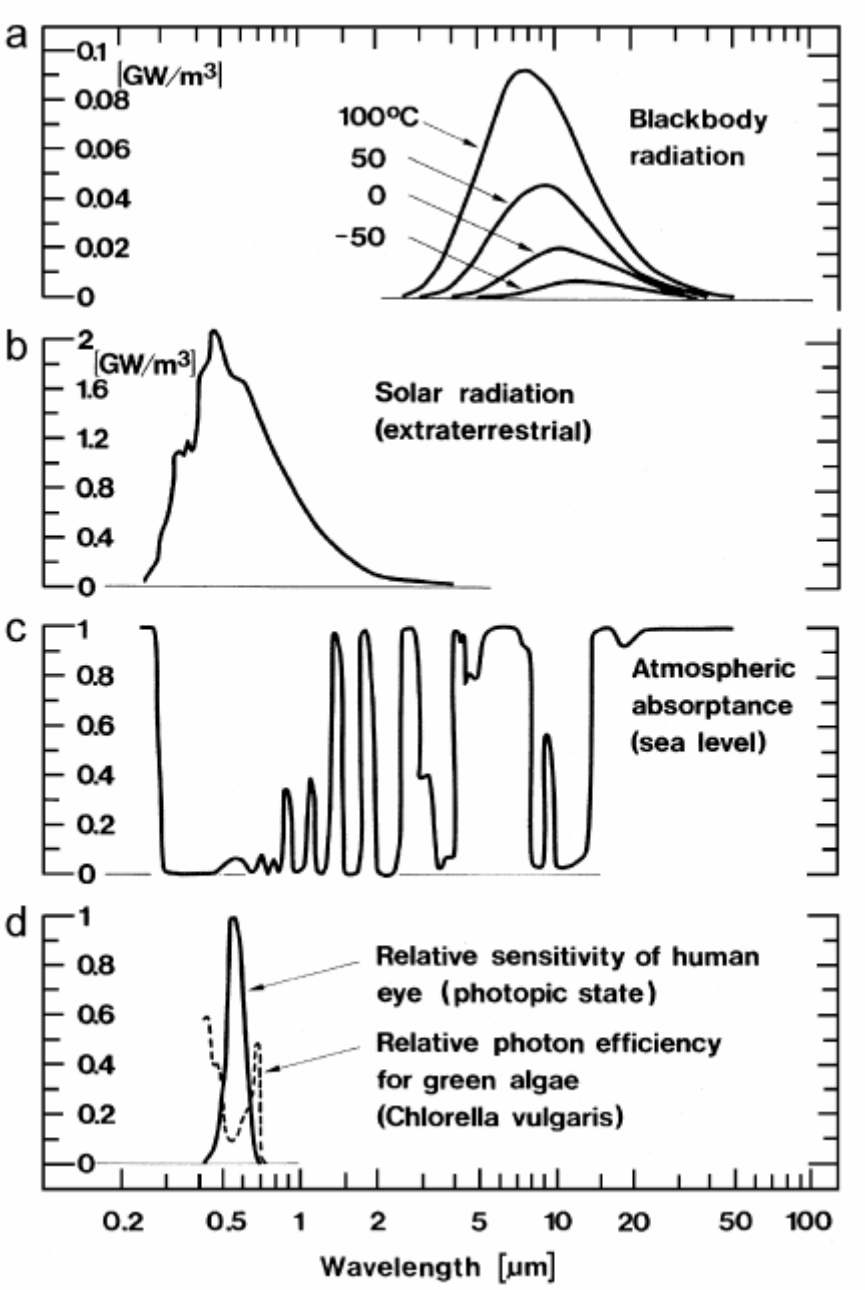

Figure 2.1: Spectra for *a)* black body radiation at four different temperatures, *b)* solar radiation outside the Earth's atmosphere, *c)* atmospheric absorptance, and *d)* relative sensitivity of the human eye versus relative photosynthetic efficiency of green algae. The latter is relevant to greenhouse applications. [5]

To set a common standard for spectrally selective windows, scientists have proposed several definitions of "the perfect window". In this regard, the location dependency and time variability of ambient conditions are essential. When analysing summer and winter separately, computer simulations have indicated the following definition of the ideal window (*Figure 2.2*):

- Summer: Only visible light is transmitted into the room; thermal radiation emitted from the indoor surfaces is transmitted to the outside.
- Winter: The entire solar spectrum is transmitted into the room; thermal radiation emitted from the indoor surfaces is reflected into the room.

Similar definitions may be applied to locations with stable hot or cold climates. To avoid radiative heat losses from the window itself, the absorptivity and emissivity should always equal zero ($\alpha_\lambda = \varepsilon_\lambda = 0$, according to Kirchhoff's law).

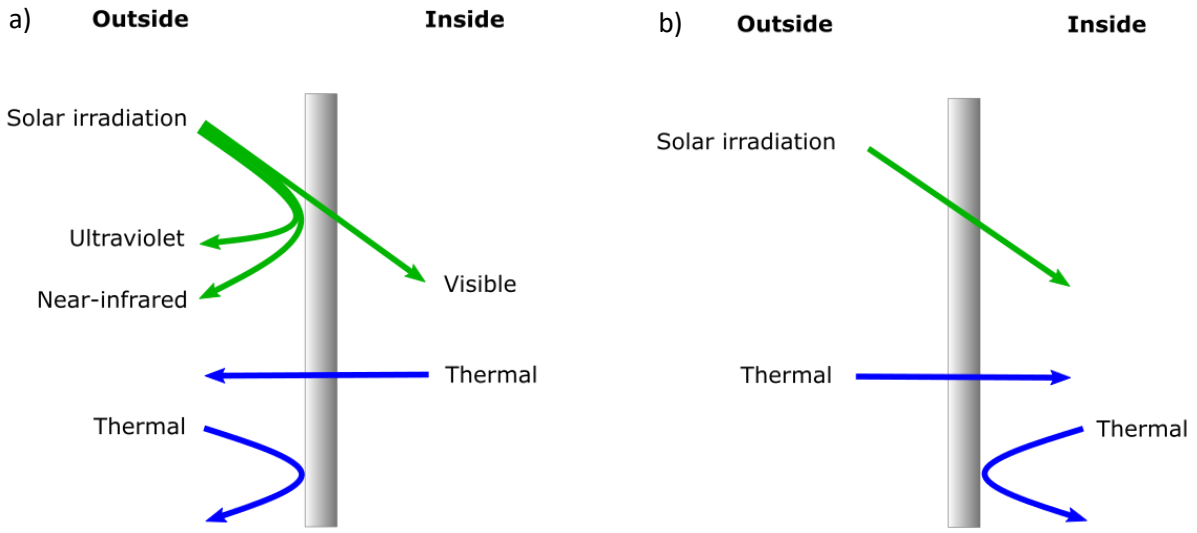

Figure 2.2: Perfect window for *a)* summer, and *b)* winter. Both windows are unidirectionally transparent to longwave thermal radiation. Adapted from[6, 7].

Currently, soda-lime glass is the most prevalent material used for windowpanes. It holds qualities such as chemical stability, workability, recyclability and low costs, but lacks the ability to regulate its infrared (IR) radiation response[8]. Normal window glass also absorbs nearly all UVB, but transmits about up to 72 % of UVA and 83 % of solar heat[9]. Furthermore, its high thermal emissivity of $\varepsilon_{th} = 0.91$ causes substantial radiative heat losses[10].

To improve the radiation control, spectrally selective coatings are often applied to soda-lime windows. The purpose of such coatings may simply be to protect against UVA, but some coatings will introduce significant energy savings. For instance, so-called *solar-control coatings* (mimicking the perfect window for summer) and *low-emissivity coatings* (mimicking the perfect window for winter) may be beneficial in warm climates and cold climates, respectively[8]. Although a step in the right direction, the big pitfall of such coatings is that they are obviously unable to respond to daily or seasonal changes. When applied in climates characterized by variable ambient conditions, static coatings may therefore *reduce* both indoor comfort and energy efficiency during parts of the year. This is where chromogenic materials are now coming to the rescue.

2.1.2 – Chromogenics

In the architectural and automotive areas, materials with the ability to undergo the process of chromism are known as *chromogenic materials*[11].There are a variety of different chromic phenomena, classified according to the stimulus that causes the colour change. Some of the most important chromisms and their stimuli are listed in *Table 2.1*, together with selected applications. Due to their commercial importance e.g. as window materials, thermo- and electrochromism will be given some extra attention below. Photochromism, being the phenomenon observed in YH_x:O, is reserved for *Section 2.2.*

Table 2.1: The six main classes of chromic phenomena, their stimuli and applications.

Phenomenon	Stimulus	Applications
Photochromism	Electromagnetic radiation	Windows, ophthalmic lenses/sunglasses, novelty and security printing, cosmetics, optical data storage, sensors, memories and switches
Thermochromism	Heat	Windows, novelty and security printing, thermometers and temperature indicators, pigments
Electrochromism	Electrical current	Windows, mirrors, displays
Solvatochromism	Solvent polarity	Analysis, sensors, monitoring of polymers and polymerisation
Ionochromism	Ions	Colour formers, thermal fax papers, indicators, metal ion detection
Mechanochromism	Mechanical friction/pressure	Biomimetic camouflage, strain sensors[12]

Electrochromic (EC) materials change optical properties according to their electronic state, i.e. the colour changes are induced by electron transfer (oxidation/reduction)[13]. The working principle of a generic EC device is somewhat similar to that of a battery: The device comprises five layers, in which an external electrical field of 1-5 V transports ions into or out of the EC layer[13]. Insertion of ions introduces electronic states within the otherwise forbidden gap, which act as colour centres[14]. This way, the IR/visible transmissivity may be adjusted by the flick of a switch[13]. Of all the chromogenic materials, EC windows are probably capable of the highest energy savings[13]. Thus, they are the most intensively studied, and already available on the commercial market[13]. However, the complexity of the technology makes it very expensive[13].

In *thermochromic (TC)* materials, optical properties vary according to temperature[11]. Both the UV and IR transmittance are switchable; the IR transmittance typically decreases as temperature increases[11]. The temperature at which the material switches from transmitting to reflecting is known as the critical temperature, T_c[11]. In the case of glazing coatings, VO_2 in the form of vanadium (IV) oxide has received the most attention, as its critical temperature ($T_c = 68$ ˚C) is the one closest to room temperature[11]. Introducing suitable dopants can reduce T_c to approximately 25 ˚C[11], but the heat received from the Sun may still not be sufficient to achieve the desired amount of darkening[15]. However, the energy-saving potential of TC windows does not lie in the materials themselves (EC materials are more effective), but in their simplicity: Single layers of TC coatings are easily combined with other energy-efficient technologies[16]. As the next section will show, simplicity is one of the great advantages of photochromic materials as well.

2.2 – Photochromism

2.2.1 – The basics

Photochromism is loosely defined as *a reversible transformation of a single chemical species between two states (A and B) having distinguishably different absorption spectra, induced in one or both directions by the absorption of electromagnetic radiation*[17]. Trivially, it can be described as a reversible colour change upon illumination. Changes may also occur in mechanical, chemical and electrical properties, such as the geometric structure, solubility, surface wettability and dielectric constants[18, 19]. The equilibrium reaction is generally represented by the equation

$$A \underset{h\upsilon_2, k_T}{\overset{h\upsilon_1}{\rightleftharpoons}} B \quad (2.1)$$

in which *A* is the initial species, *B* is the photoproduct, *hν* is the photon energy and k_T is the thermal bleaching rate constant[17]. Note, however, that some reactions are multimolecular. In most cases, A will absorb in the UV or near-UV part of the spectrum[20], but depending on the material, the transformation may be triggered by UV, visual or IR radiation[17]. The reverse reaction ($B \rightarrow A$) is thermally and/or photochemically induced, by which the systems are distinguished as either *T-type* or *P-type*, respectively.

Photochromism was first reported in tetracene solution in 1867[20]. Today, the phenomenon has been observed in numerous organic and inorganic materials, plus some biological systems[18]. Organic photochromism is both the most common and the most extensively explored group of systems[21]. However, inorganic materials have some advantages over organic materials, such as thermal stability, chemical resistance, strength and workability[22]. Inorganic photochromic substances exist as thin films, crystals, thermoplastics, segnetoelectrics and glasses[23]. In the case of thin-film technology, transition metal oxides (e.g. TiO, MoO_3, WO_3 and YH_x) are particularly interesting[24], as they offer a large flexibility to tune the photochemical and photophysical properties[21]. An example of photochromic sunglasses is shown in *Figure 2.3;* These glasses have been commercially available since 2007[25].

Figure 2.3: Photochromic glasses subjected to three different lighting conditions. Visual and UV radiation triggers rearrangements of the photochromic molecules, causing the colour to change from yellow/green, via copper, to reddish brown according to the radiation intensity. The lenses are also polarized by an angularly selective thin film. Adapted from [25].

2.2.2 – Reaction mechanisms

Some of the most prevalent photochromic reaction mechanisms are listed in *Table 2.2.* Inorganic materials are dominated by (intervalence) charge transfer processes, in which redox reactions create defect bands[26-28]. Such defects typically consist of vacancies with the ability to trap electrons[29]. This appears visually as an absorption peak in what would otherwise be a transparent (sub-bandgap) part of the spectrum[26, 27]. Additionally, various intermediates and side reactions may be involved, determining the efficiency and cyclability of the reaction. In the following, we will only be concerned with simple $A \rightleftarrows B$ photochromic systems.

Table 2.2: Common photochromic mechanisms[30, 31].

Rearrangement processes		Dissociation processes	
Isomerisation:	A* → B	…into ion and electron:	A* → $A^+ + e^-$
Charge Transfer		…into two ions:	A* → B+ + C–
Hydrogen transfer		…into stable molecules:	A* → B + C
		…into radicals:	A* → B● + C●

The nature of the photochromic interconversion depends on the initial energy of the molecule, and on the geometry of the potential energy surfaces (PES)[17]. As *Figure 2.4* illustrates, *A* and B are separated by a potential barrier known as the activation energy, E_a. In a system of potential reactants, the activation energy is defined as the minimum energy required to initiate a reaction. More precisely, it is the energy needed to contort the molecule into the transition state, in which the molecular bonds are able to break. The activation energy is normally quite high in the ground electronic state ($E_a \approx 0.867\ eV$), and low/non-existing in the exited state[32]. Thus, the conversion of reactants into products is far more likely in the exited state than in the ground state[32]. As a result, photochromic reactions often consist of both photophysical processes (which alter the electron density distribution) and photochemical processes (which reorder the atoms, corresponding to changes in the PES of the molecule)[17].

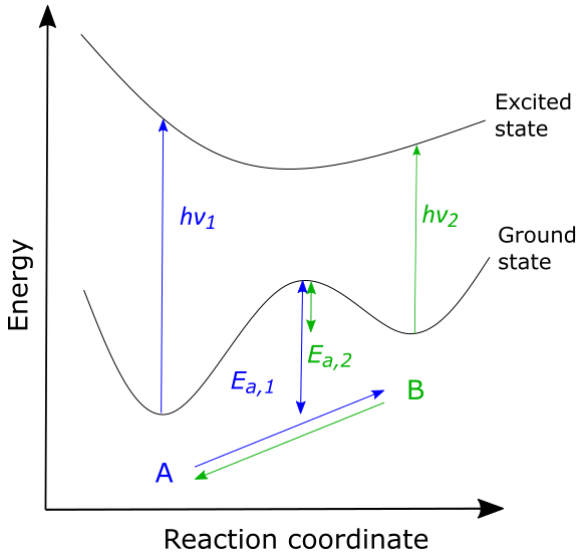

Figure 2.4: Reaction coordinate of positive, photoreversible photochromism. E_a denotes activation energy, hv is photon energy. Adapted from [20]

Photophysical processes

When a photochromic material is illuminated by EM radiation, photons are either absorbed, transmitted or reflected. Only absorbed photons can contribute to the photochromic reaction. Since defect-free semiconductors exclusively absorb photon energies higher than the band gap energy, such materials will experience a sharp rise in the absorption spectrum at the wavelength corresponding to the band gap. *Most inorganic solids exhibiting photochromism have large optical band gaps of 3 eV < E_g < 12 eV, corresponding to wavelengths 100 nm < λ < 400 nm[33]. This entails a negligible absorption in the visible* part of the spectrum (*400 nm < λ < 700 nm*, *Figure 1.1*).

Upon absorption of photon energies in the far IR, NIR/IR or visual/UV, *A* is excited from the ground state to a rotational, vibrational or electronic excited state (*A**), respectively[30]. Subsequently, *A** will either react to form *B*, or deactivate to its ground state (*A*) by thermal relaxation, fluorescence or non-radiative decay. Normally, only the electronic excited states possess enough energy to cause reactions[30].

Photochromic systems are referred to as either *positive* or *negative*. Positive photochromism, which is the most common of the two, involves a colourless (or pale yellow) substance acquiring colour through a monomolecular reaction. If the system is photoreversible, the initial species *A* will absorb at shorter wavelengths than the photoproduct *B*, with a characteristic absorption band at $\lambda_1[A] < \lambda_2[B]$. The absorption spectra of positive photochromism is illustrated in *Figure 2.5*. In the case of negative photochromism, a coloured substance becomes transparent due to a bimolecular reaction. The initial species will then absorb at longer wavelengths than the photoproduct: $\lambda_1 > \lambda_2$.

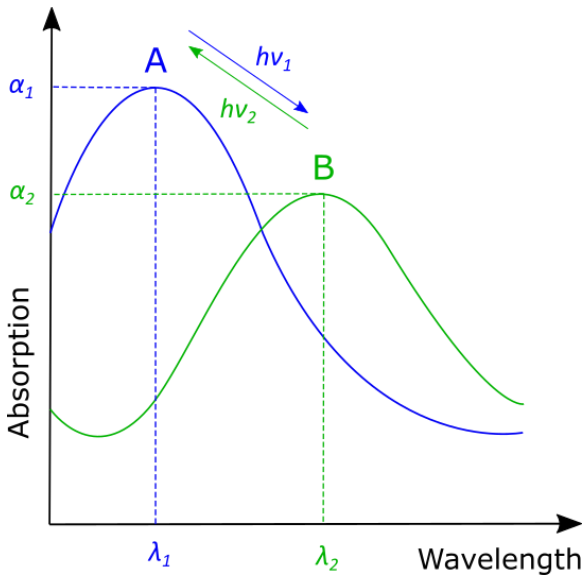

Figure 2.5: Absorption spectra of positive, photoreversible photochromism. Adapted from [20].

Photochemical processes

Three different classes of photochemical reactions may be distinguished, based on their pathway through the PES (*Figure 2.6*)[17]. The most common mechanism in organic materials is the *diabatic photoreaction (a)*, in which the excited *A** converts directly into ground state *B*[17]. Because there is essentially no thermal barrier between *A** and *B*, and because the decay happens so fast, this pathway is temperature independent. Diabatic reactions may occur if the ground state PES is relatively close to the excited state PES[17]. A second interconversion pathway is represented by *adiabatic photoreactions (b)*. In such a reaction, *A** converts to *B* via the excited *B**, whose minima is preferably lower than that of *A**[17]. Also, the exited states are separated by a (relatively low) thermal barrier, meaning that the equilibrium of the reaction can be controlled by changing the temperature. The third and final pathway is the "*hot" ground state photoreactions (c)*, in which *A** returns to its ground state with enough excess thermal energy to cross the barrier between *A* and [17]*B*.

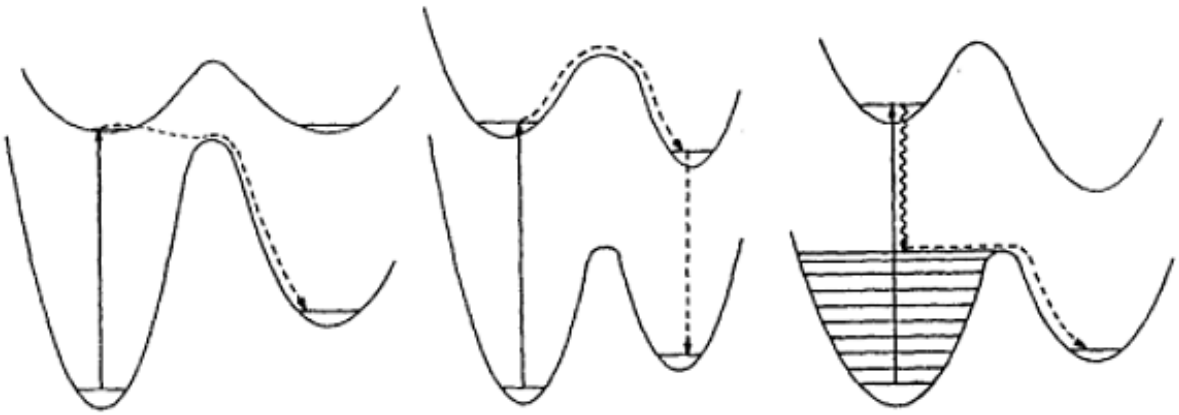

Figure 2.6: (a) Diabatic photoreactions, *(b)* adiabatic photoreactions, *(c)* "hot" ground state photoreactions[17].

Naturally, the PES will also influence the backreaction $B \rightarrow A$. In a thermoreversible system, the potential barrier separating *A* and *B* is low enough for *B* to revert spontaneously to *A*[20]. Hence, adiabatic forward-reactions are followed by quite fast thermal back-reactions, as the low energy barrier in the exited state is accompanied by a relatively low barrier in the ground state[17]. A photoreversible system, however, requires additional energy from photons to induce the backreaction[20].

2.2.2 – Kinetics

The course of a reaction $A \rightarrow B$ is generally given as the rate at which the reacting material A is consumed. In the case of photochromic systems, concentrations may be indirectly monitored using time-resolved spectrophotometry – as will be explained in *Chapter 3*.

If the $A \rightarrow B$ reaction rate is constant, it is expressed by a zeroth order differential equation:

$$\frac{da}{dt} = -k \quad \left[\frac{moles}{dm^3 s}\right] \quad (2.2)$$

where a is the concentration of A and k is the reaction rate constant[34]. *Equation 2.2* is applicable e.g. to photochemical reactions in which the light intensity is constant and rate determining[34]. If, however, the reaction rate is directly proportional to the concentration of A, the reaction is said to be of first order[34]. This gives the general representation of most thermal reactions:

$$\frac{da}{dt} = -\mathrm{k}_t a \quad \left[\frac{moles}{dm^3 s}\right] \quad (2.3)$$

with k_t being the thermal rate constant[30], which depends upon the temperature and activation energy according to the *Arrhenius equation:*

$$k_t = Ae^{-E_a/RT} \quad [\mathrm{s}^{-1}] \quad (2.4)$$

where T is temperature, R is the universal gas constant, and A the frequency factor (the latter indicates the frequency of collisions in the direction that will cause a reaction)[35]. In the equivalent case of a photoreaction, the rate depends on the amount of light absorbed, which in turn depends on the changing concentration of A[30]. Therefore, the photochemical analogy to *Equation 2.3* is

$$\frac{da}{dt} = -\varphi I_A \quad \left[\frac{moles}{dm^3 s}\right] \quad (2.5)$$

where φ is the quantum yield, and I_A is the time-dependent amount of light absorbed by A[30]. The quantum yield is the number of reactions $A \rightarrow B$ per photon absorbed[30]. Alternatively, φ may be interpreted as the probability that the absorbed photon will yield B, as opposed to thermal relaxation, fluorescence or non-radiative decay:

$$\varphi = \frac{k_r}{k_r + \sum k_d} \quad [-] \quad (2.6)$$

with k_r being the rate constant of the photochromic reactions, while Σk_d represents all unwanted processes that cause deactivations[30]. If correctly defined, the quantum yield is a time-independent constant[30]. The light absorbed by A can be expressed as

$$I_A = I_0 \varepsilon'_A F'(t) a \quad \left[\frac{moles\ of\ photons}{dm^3 s}\right] \quad (2.7)$$

where I_0 is the incident intensity, ε' is the molar absorption coefficient, a is the concentration of A, and F' is the photokinetic factor at irradiation wavelength λ' and time t (the latter represents the fraction of total absorption which is due to component A)[30].

At the *isosbestic point*, defined as the wavelength at which *A* and *B* have the same absorbance, the photokinetic factor is constant[36]. As a result, *Equation 2.5* reduces to a general first-order reaction:

$$\frac{da}{dt} = -\mathrm{k}_{p,app}a \quad \left[\frac{moles}{dm^3 s}\right] \quad (2.8)$$

in which a is the concentration of *A*, and $k_{p,app}$ is the apparent rate constant of the photoreaction:

$$k_{p,app} = \varphi I_0 \varepsilon'_A F' \quad [s^{-1}] \quad (2.9)$$

where φ is the quantum yield, I_0 is the incident intensity, ε' is the molar absorption coefficient, a is the concentration of *A,* and *F'* is the photokinetic factor[36].

Recall that thermal reactions may be superimposed on photoreactions in one or both directions, and that the forward and backward reactions may occur at the same time. For instance, a two-species system with a photoinduced forward reaction and a thermal backward reaction – known as an (*AB, 1φ, 1k)* system – would be represented as

$$\frac{da}{dt} = -\frac{db}{dt} = -\varphi I_A + \mathrm{k}_t b \quad \left[\frac{moles}{dm^3 s}\right] \quad (2.10)$$

where a is the concentration of *A, b* is the concentration of *B*, φ is the quantum yield of the photoreaction, I_A is the amount of light absorbed by *A*, and k_t is the rate constant of the thermal reaction[30]. At the isosbestic point, the photodarkening rate and the bleaching rate would be

$$k_{darkening,app} = k_{p,app} + k_t \quad [s^{-1}] \quad (2.11a)$$

$$k_{bleaching} = k_t \quad [s^{-1}] \quad (2.11b)$$

in which $k_{p,app}$ is the apparent rate constant of the photoreaction, as given in *Equation 2.9*[36]. At the *photostationary state (PSS)*, the bleaching rate exactly equals the darkening rate; Consequently, the absorbance of the coloured form is constant[36]. The PSS may be used as a measure of the system's practical interconversion efficiency. Its position depends on irradiation parameters (e.g. wavelength), the absorption spectra of A and B, and the quantum yields of the reactions[30].

It is not unusual for the observed darkening and bleaching curves to exhibit an apparent mono-exponential form, the solution of which is given by the equation

$$a(t) = a_0 e^{-t/\tau} \quad \left[\frac{mol}{dm^3}\right] \quad (2.12)$$

where a_0 is the initial concentration of *A* at time $t = 0$[30]. τ is the mean lifetime of molecule *A:*

$$\tau = \frac{1}{k} \quad [s] \quad (2.13)$$

where k is the rate constant[30]. Thus, the challenge of kinetic analysis often consists in unravelling a set of fitted exponential equations into their constituents. From the above discussion, it is evident that the level of difficulty in doing so, may lie anywhere between 'fairly straightforward' and 'rather cumbersome'.

2.3 – Oxygen-containing yttrium hydrides (YH_x:O)

In 1996, Huiberts *et al.* discovered the gasochromic properties of yttrium hydride (YH_x) thin films, and its application was named "the switchable mirror"[37]. Five years later, Hoekstra et al. reported persistent photoconductivity at low temperatures[38]. Ohmura *et al.* then followed with the observation of photochromic behaviour in yttrium hydride films subjected to high hydrogen (H_2) pressures[39]. The next big advancement was made in 2011 by Mongstad *et al.*, who accidentally discovered the photochromic effect in oxygen-containing yttrium hydride films (YHx:O) at ambient conditions[28].

2.3.1 - YH_x

Yttrium hydride is generally classified as a rare-earth metal hydride, whose switchable optical properties can be tuned by changing the hydrogen concentration[29]. YH_x may be observed in three different phases at room temperature and atmospheric pressure: the *hcp* α-phase (Y containing small, dissolved amounts of hydrogen), the *fcc* β-phase (the dihydrides, YH_2) and the *hcp* γ-phase (the trihydrides, YH_3)[40, 41]. While the dihydrides are metallic and shiny, the trihydrides are semiconducting and transparent to visible light[37]. The transition is caused by the opening of an indirect band gap close to 3 eV[42], which is simply induced by changing the surrounding H_2 pressure or electrolytic cell potential[37]. At a total pressure of 5.8 GPa (~57000 atm), transparent YH_x is observed to darken when illuminated by a 488 nm laser with an intensity of 10^5 W/cm^2 (~10^6 times normal solar irradiation)[39]. Further increasing the pressure to 23 GPa will induce a *hcp-fcc* phase transition in YH_3, accompanied by the closure of the electronic band gap and a corresponding drop in the transparency[43, 44].

2.3.2 – YH_x:O

The photochromic properties of YH_x drastically change upon the incorporation of oxygen[28]. In 2011, Mongstad et al. reported that transparent YH_x containing ~5-30 % oxygen exhibits a colour-neutral darkening when illuminated by moderate light intensities (~0.1 W/cm^2) at ambient conditions[28]. Both visible and UV radiation induced the transition, but the reaction was strongest with photon energies exceeding the band gap of ~2.6 eV (e.g. blue light)[28]. The transmission in the visible and IR domain was reduced by up to ~50 % after one hour of illumination, and returned to the initial state when left in the dark[28]. The recovery time depended on sample temperature, illumination intensity and illumination time[45]. Pictures of a sample before and after illumination is included in *Figure 2.7* (next page); The initial yellow colour is due to absorption of blue and violet light by band-to-band excitations[28].

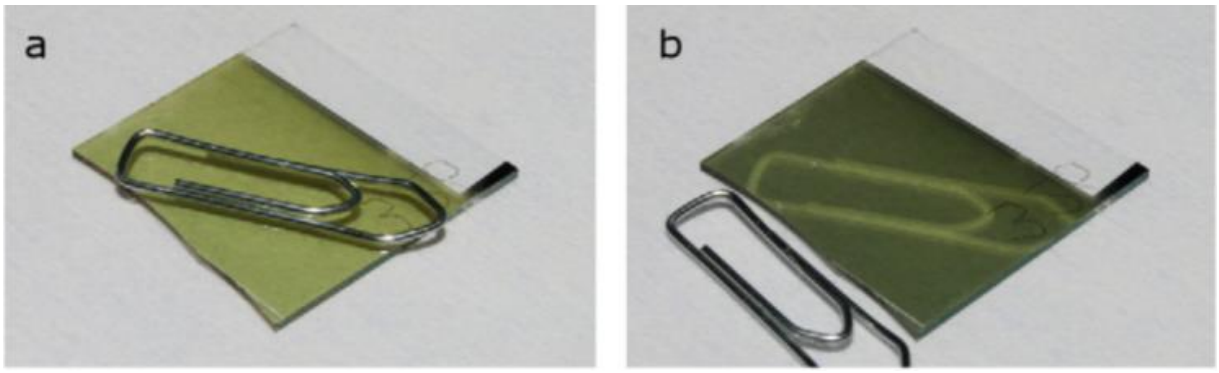

Figure 2.7: A 550 nm thin film of YH_x:O *(a)* before and *(b)* after one hour of illumination by a solar simulator. The sample was covered by a paperclip during the illumination for illustrational purposes.[28]

Synthesis

Photochromic YH_x:O can be synthesized by allowing sputter deposited YH_x to react with air[46]. The process of magnetic sputter deposition will be thoroughly explained in *Chapter* 3. In short, it involves the deposition of metallic Y onto a substrate in a hydrogen-containing atmosphere (typically an H_2/Ar mix). Samples prepared at high [H_2]/[Ar] ratios are observed to hold a high amount of oxygen[47, 48]. This is currently explained by the porous structure of samples deposited at high H_2 partial pressures, as the oxidation upon exposure to air is known to happen through pores and holes[47-49]. Indeed, increasing the time of air exposure has been shown to increase the oxygen content through gradual oxidation of the samples[50]. So far, the highest oxygen-to-yttrium ratio reported is *[O]/[Y] = 1.67*[45].

In a recent optical experiment, the as-deposited film transformed from dark/opaque/metallic to yellowish/transparent/photochromic upon reaction with oxygen in air[46]. The initial substance was assumed to be YH_2, because it exhibited an *fcc* structure with a lattice parameter equal to the one earlier reported for YH_2 ($a = 5.2$ Å)[46, 51]. The structure remained *fcc* during the transition, indicating that oxygen stabilizes the *fcc* phase at ambient pressure (as transparent, oxygen-free YH_2 only appear in a *fcc* structure at high pressures). At the same time, the lattice parameter increased to $a = 5.4$ Å[46, 48, 52, 53]. This lattice expansion has been observed in oxygen-containing samples several times, justifying the assumption that it is in fact a result of the oxygen being incorporated into the lattice[48, 52, 53].

Reaction mechanisms

It has been postulated that the photochromic reaction in YH_x:O_w can be explained quantitatively by the gradual growth of metallic YH_y:O_z domains within the initial semiconducting lattice upon illumination[48]. The metallic domains contain only small amounts of oxygen, and are able to absorb sub-bandgap wavelengths[48]. Even small amounts of these domains may considerably reduce the optical transmittance: A volume fraction of $f = 0.02$ occupied by the metallic phase was shown to cause a >30 % decrease in the visible spectrum[48]. The domains were assumed to be much smaller than the wavelength of the incident radiation, and thus the photodarkened material should behave optically like a homogenous medium[48].

The absorption of photons close to the band gap energy (E_g) is probably essential in the photochromic reaction, seen as it appears to be greater before than after photodarkening[54]. Also, the increased photodarkening observed at photon energies above E_g indicates the importance of charge carrier generation[28]. The same can be concluded from the persistent photoconductivity accompanying the photochromism[28]. However, upon illumination by photon energies exceeding the band gap, the transmittance of the material changes to a constant value at wavelengths above the fundamental absorption edge. This indicates that the photochromism does not involve localized defects due to redox reactions[26]. Furthermore, X-ray diffraction studies have revealed a lattice contraction due to structural rearrangements during illumination[26]; This suggests that the photochromic reaction is not driven by a purely electronic mechanism[54]. One hypothesis is that the absorption of photons causes rearrangements of the lattice, by shifting H and/or O atoms from their initial locations – which in turn triggers a contraction of the lattice[26]. This is supported by the mobile hydrogen fraction which is released from the lattice upon illumination, and subsequently reabsorbed when left in the dark[50, 55].

The exact role and location of oxygen in the lattice is still unclear[48]. Theoretical simulations have indicated that the high electronegativity of oxygen causes charge transfers, through replacement of hydrogen by oxygen (*Figure 2.8*)[53]. Generally, increasing the oxygen content shifts the absorption band edge towards shorter wavelengths. The direct optical band gap increases accordingly, from the mentioned $E_g = 2.6\ eV$ in oxygen-free YH_3, to $E_g = 2.8\text{-}3.7\ eV$ at corresponding deposition pressures $P_{tot} = 0.4\text{-}6.0\ Pa$[54, 56]. This may be seen in connection to the oxygen-dependent electron momentum distribution[29]. As a result, the reaction is mostly triggered by UV radiation in samples which are rich in oxygen, whereas the samples with lower [O]/[Y] ratios respond to both visible and UV radiation[54]. A greater band gap will thereby reduce the number of useful photons absorbed, which might be the cause of the weakened photodarkening reported at high oxygen contents[54].

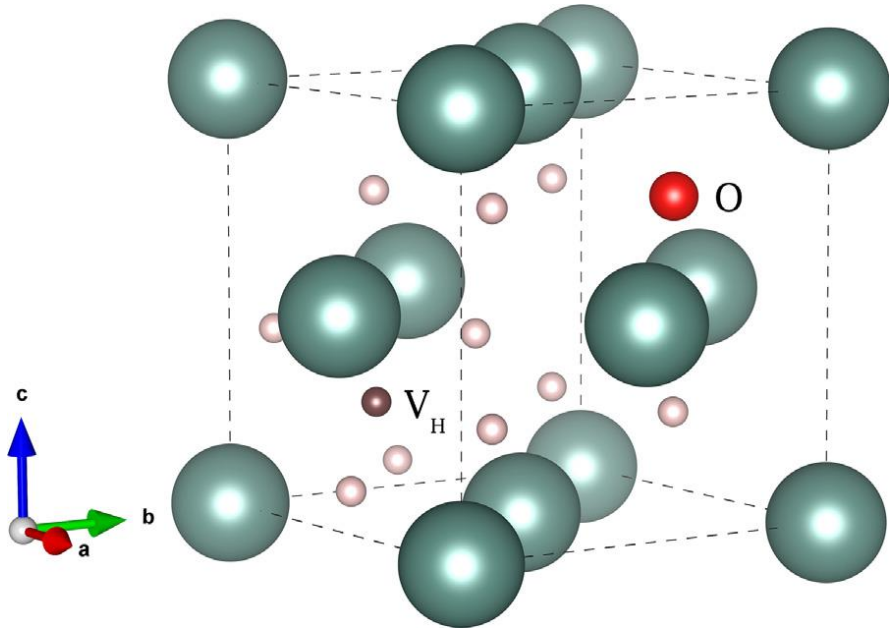

Figure 2.8: Schematic illustration of the fcc $YH_{2.5}O_{0.25}$, as indicated by theoretical simulations[53]. Turquoise spheres represent Y atoms; beige sphere represent H. Two H atoms are replaced by O (red sphere); the vacancy left by one of them is depicted by the brown sphere.

Kinetics

A typical plot of the time-resolved transmission of YH_x:O is presented in *Figure 2.9*. As can be seen from the plot, the reaction rates are somewhat low – similar to those observed in transition metal oxides[28]. The bleaching reaction is noticeably slower than the darkening reaction. More specifically, the bleaching examined by Mongstad in 2011 was reported to take several hours, depending on the duration and strength of the illumination[45]. After one day of exposure to sunlight, the bleaching could take up to several days[45]. However, Mongstad also observed that heating the material to 40-50 °C greatly increased the bleaching rate[45]. Whether or not this is due to a useful (and possibly tuneable) activation energy, is yet to be established.

Although the photodarkening happens at a higher rate than does the thermal bleaching, Mongstad did not obtain a photostationary state even after several hours of illumination.[45] The quickest photodarkening appeared to occur in the samples containing the least oxygen[45]. Furthermore, recent research has indicated that coating the YH_x:O with a WO_3 capping layer may be another way of increasing the colouration rate. It should also be mentioned that a memory effect has been observed in areas of the material that have previously been exposed to light[28]. This memory effect causes faster photodarkening and slower thermal bleaching for several weeks after the previous light exposure[28, 29].

A proper understanding of reaction kinetics is essential in the field of photochromism. Although the preliminary findings mentioned above provide helpful hints, a thorough analysis is necessary to gain applicable knowledge. With that in mind, the work in this project will be inspired by Mongstad's observations regarding ambient conditions.

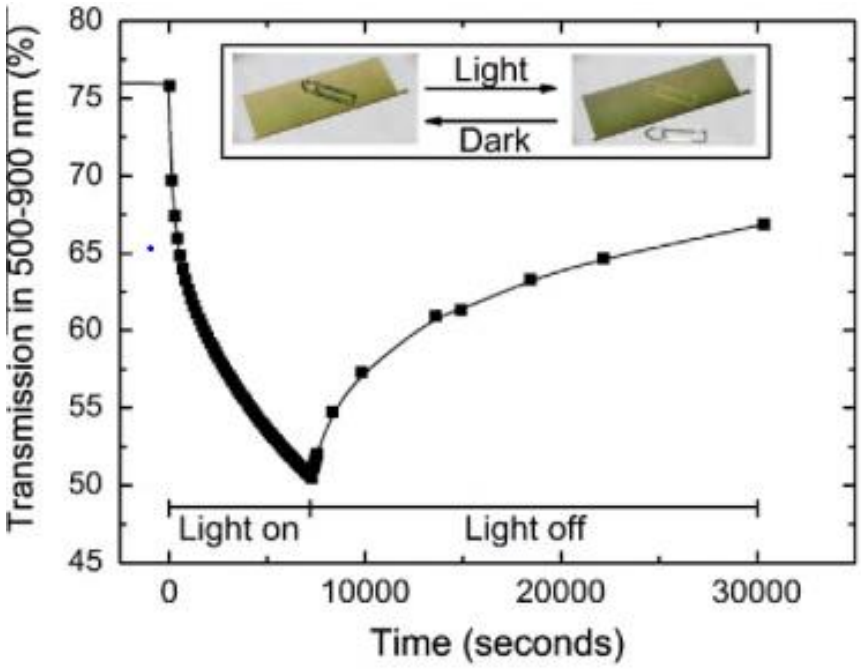

Figure 2.9: A typical plot of the time-resolved transmission of an YH_x:O thin film, during photodarkening and bleaching[26, 45]. In this experiment, the photoreactions were induced solely by the probe light of the transmission measurement equipment itself – indicating the difficulty of performing objective measurements of photochromic systems.

3. Methods

3.1 – Synthesis: Reactive DC magnetron sputtering

Photochromic YH_x:O is synthesized using so-called *reactive magnetron sputtering*. Magnetron sputtering is a vacuum deposition technique for producing thin films or coatings of metals, alloys and compounds[57]. It is a physical vapor deposition process, in which atoms or molecules are vaporized from the target material, and then recondense onto a solid substrate (typically glass, polymers, metals, etc.)[58, 59]. To avoid delamination of the films, substrates must be thoroughly cleaned prior to the sputtering.

Conducting materials are normally deposited using a *direct current (DC)* sputtering system, the working principles of which are illustrated in *Figure 3.1*. In a DC sputtering system, the target is connected to a cathode, while the substrate and chamber walls are grounded[16]. The chamber is filled with an inert gas, normally argon (Ar). During sputtering, an electric field ranging from a few hundred to a few thousand eV accelerates free electrons from the cathode towards the positive electrode[58]. Upon collision with Ar atoms, the electrons ionize the Ar gas into a plasma. Ar^+ ions are then accelerated into the negatively charged target, creating sputtered atoms and secondary electrons[58]. Finally, sputtered atoms may impinge on the substrate, provided sufficient energy and mean free path[58].

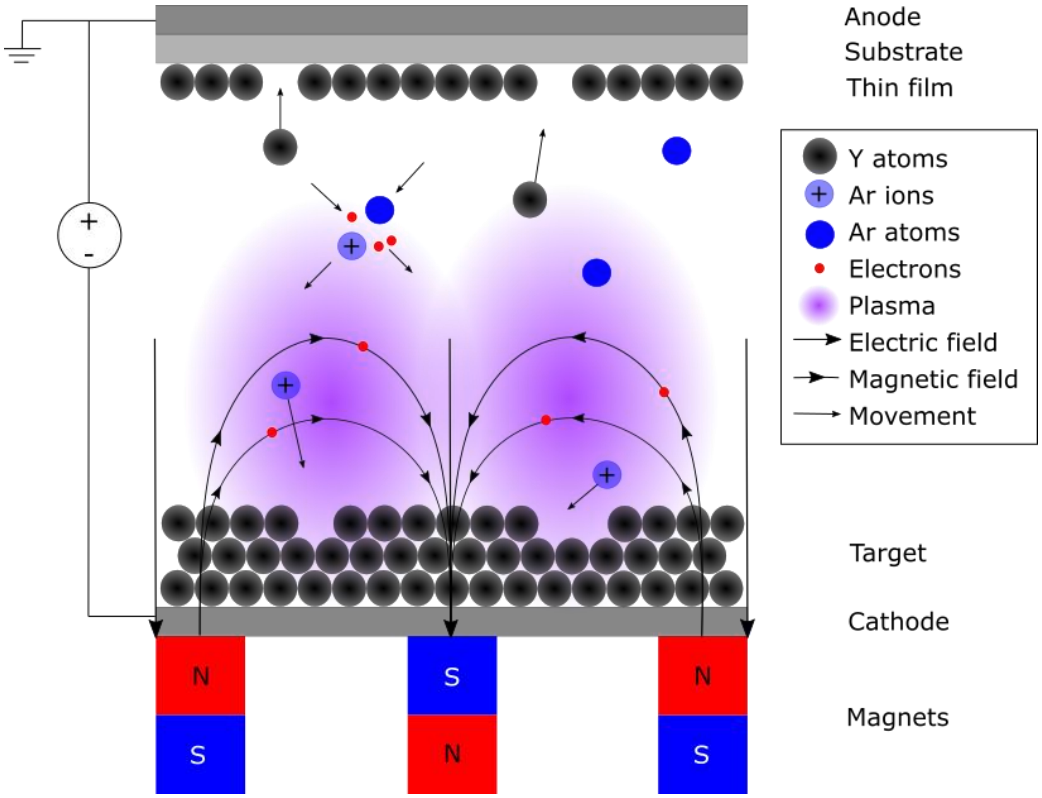

Figure 3.1: Working principles of reactive DC magnetron sputtering. Inspired by [60, 61].

Adding reactive gases to the inert gas produces compounds as the final product, and is termed *reactive* DC sputtering[16]. The mixing ratio is of great importance: Recall that YH_x deposited at a high H/Ar ratio is found to exhibit a stronger photochromic effect. When dealing with an insulating target, as may be the case for yttrium at high hydrogen injection levels, charge tend to build up on the target surface[28]. To discharge such voltage buildup, the sputtering power is often applied in periodic pulses, thereby preventing the occurrence of arcs[62].

To increase the deposition rate and reduce the pressure necessary for plasma generation, *magnetrons* are often applied to the sputtering systems. Magnetron sputtering utilizes magnetic fields to confine electrons in closed *E x B* drift currents in front of the target. In addition to preventing energetic electrons from damaging the substrate, these "traps" increase the mean free path of the electrons[58]. This in turn enhances the probability of ionization by several orders of magnitude, and creates a uniform deposition layer[58].

Experimental

In this project, photochromic thin films of YH_x were deposited onto six soda lime glass substrates, a schematic is presented in *Figure 3.*2. Prior to the sputtering, the substrates were prepared in a cleanroom (using acetylene, ethanol, deionized water and woven wipes). The films were synthesized by reactive magnetron sputtering from a 99.99 % pure metallic yttrium target in a Leybold Optics A550V7 in-line sputtering system, operated at a DC power of 1000 W. The power was pulsed at frequency of 70 kHz, with a reverse cycle of 4.0 µs. To ensure an even deposition layer in the sample region, the substrate table was set to oscillate horizontally with a speed of 3 m/min and an amplitude of 0.5 m. The sputtering was performed in an argon-hydrogen atmosphere at the following conditions: base pressure $2.3*10^{-3}$ mbar, deposition pressure $8.3*10^{-3}$ mbar, H_2/Ar-flow ratio 23sccm/160sccm, and gas purities 5N.

Afterwards, the samples were exposed to air to ensure incorporation of oxygen. To allow the material to stabilize, the samples were stored in sealed plastic bags (containing air) for approximately three weeks before initiating any experiments.

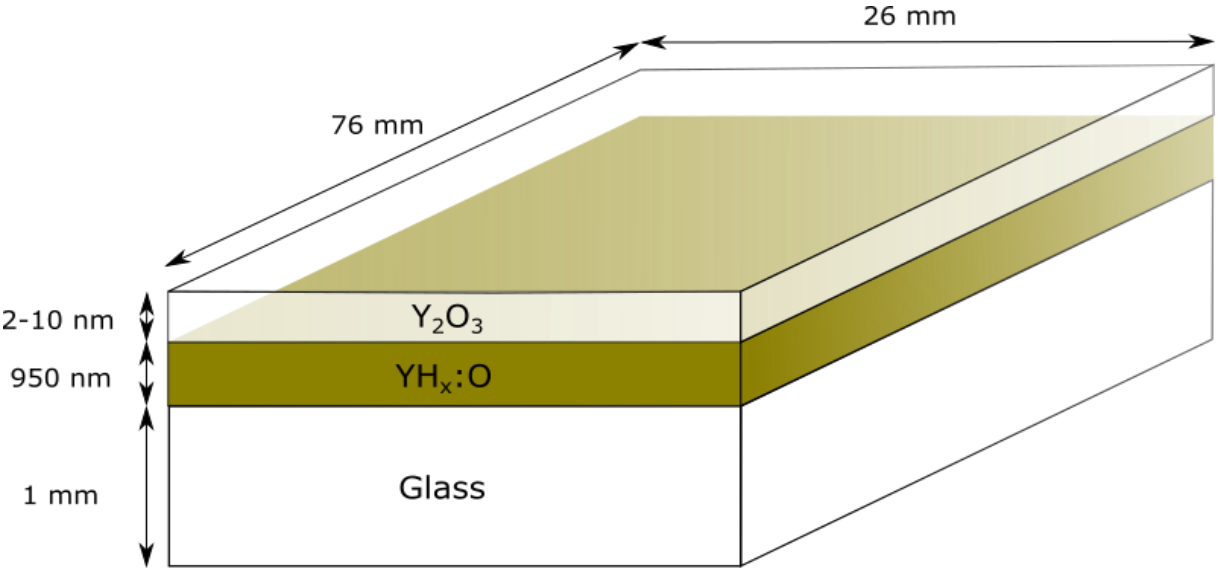

Figure 3.2: Schematic of a YH_x:O thin film sample (with surface oxide layer) on glass substrate.

3.2 – Optical measurements

This project will investigate how the photochromic behaviour of YH_x:O is effected by the following three parameters: sample temperature, incident radiation intensity, and incident radiation wavelength. The photochromic response is monitored by transmission spectrophotometry.

The general setup for the main experiments is illustrated in *Figure 3.3*: The samples were illuminated by an Energetiq EQ-99XFC LDLS broad band light source with an intense UV component, and the transmittance was measured in-situ by Ocean Optics QE6500 and NIRQUEST512 spectrometers equipped with a Newport 4-port integrating sphere. The integration time (which is analogous to the shutter time of a camera) was set according to the irradiative power in each experiment. Prior to the experiments, the equipment was allowed to stabilize for at least 30 minutes. A rotatable low-transmittance filter (situated between the sample and the light source) was used to initiate/terminate the illumination of the samples.

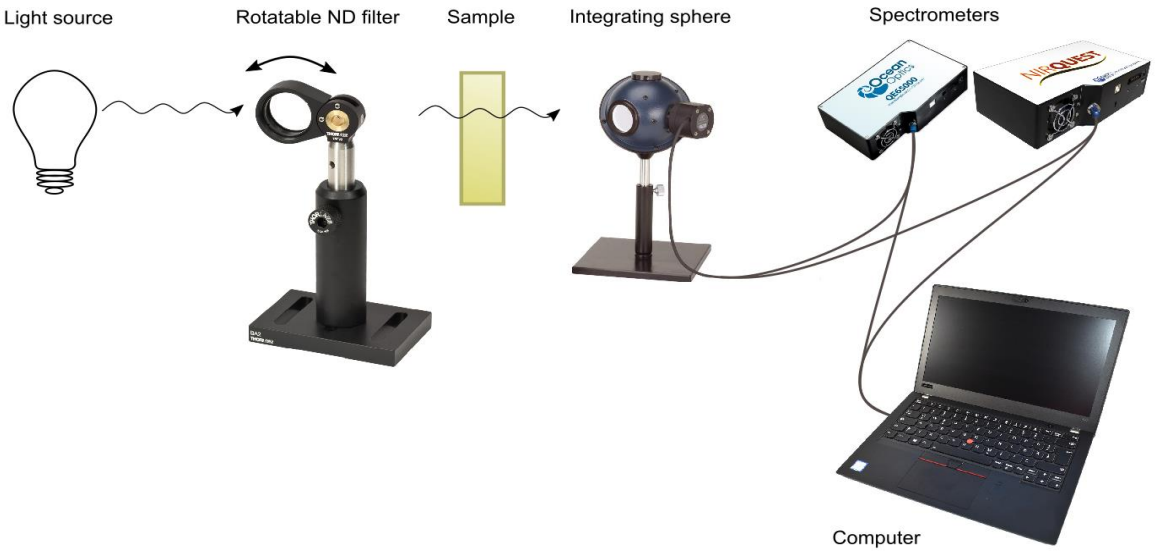

Figure 3.3: General setup for main experiments[63-67].

The data acquisition was performed using the Ocean Optics OceanView software. Each recording contains the transmission spectra in the wavelength interval $198 < \lambda < 998$ *nm*. However, unless otherwise stated, the transmission given as a function of time is the average transmission during the interval $500 < \lambda < 900$ *nm*. This averaging was performed to exclude less interesting and less accurate wavelengths.

All measurements were performed in a dark room, though some light pollution was inevitable. The light pollution – as well as other undesired contributions to the recorded spectra – was accounted for by defining irradiation baselines in the Ocean Optics software before each experiment.

Note that one sample was needed per measurement, meaning that all samples were used several times. Each sample is referred to by a sample number 1-6, followed by a number indicating the number of times the sample has been used in a photodarkening experiment. Between each experiment, the samples recovered in sealed plastic bags (containing air) stored in the dark for at least 78 hours. To avoid the memory effect, different parts of the samples were illuminated each time.

3.2.1 – Initial measurements

Initial values of the sample thickness, reflectance and transmittance were recorded prior to the experiments. The thickness was determined by *contact profilometry*, in which a probe is moved along a sample surface while monitoring the force from the sample on the probe.

The setup used for measuring reflectance and transmittance was similar to that of *Figure 3.4*. To avoid photodarkening of the samples, the light source applied in this setup (an Ocean Optics DH-2000) was weaker than the one described in the general setup. As a result, a different integrating sphere (an Ocean Optics ISP-R) was also needed. Calibration was performed with a Labsphere USRS-99-010 reflectance standard.

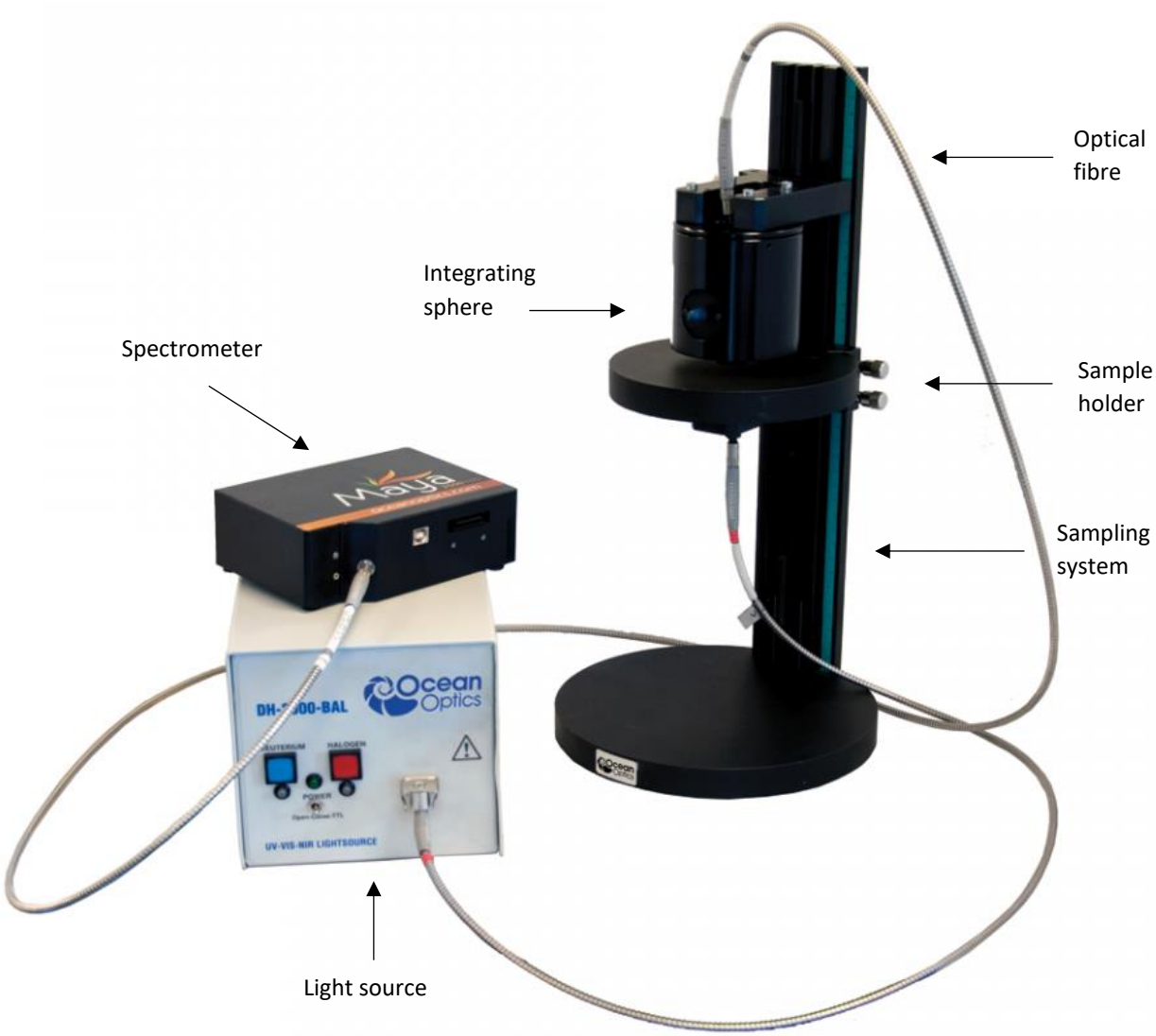

Figure 3.4: Transmittance measurement setup[68]. In the case of a reflectance measurement, both optical fibres are connected to the integrating sphere. In both cases, the sample is placed so that the film faces the light source, i.e. the red optical fibre.

3.2.2 – Temperature measurements

To investigate the effect of sample temperature on the photochromic effect (PCE), the samples were heated above room temperature with a blow dryer. The blow dryer had three different heating levels, which were applied at different distances from the sample. The sample temperature was monitored with a thermocouple connected to a multimeter, and a rotatable low-transmittance filter was used to terminate the photodarkening. *Figure 3.5* illustrates the setup.

Because a heating experiment has never been performed on YH_x:O before, part of the goal was to investigate the possibilities and limitations of the available equipment and procedures. Hence, the experimental methods were planned and refined along the way, resulting in three different procedures:

1. Initial experiment to quickly establish whether there is an obvious effect of temperature on the PCE in the samples (and to check that the improvised set-up was reliable).
2. Heating of samples during thermal bleaching only, in order to isolate this process as much as possible, and to investigate the dynamics between sample temperature and photochromic response.
3. Preheating of samples to stable temperatures before initiating illumination, to avoid the dynamics of heating. Illumination to a pre-decided transmittance, to avoid possible effects of initial transmittance on the bleaching kinetics. The temperature was kept ~constant throughout the experiment.

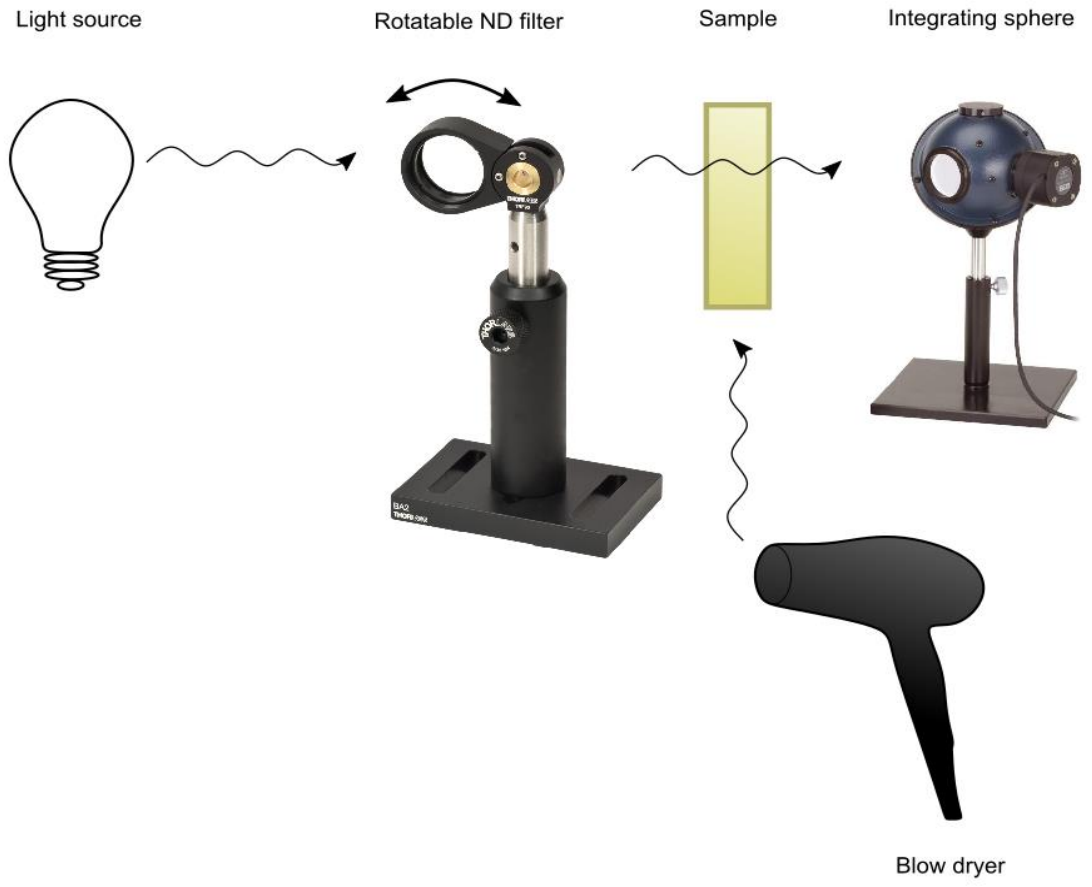

Figure 3.5: Setup for temperature experiments[63, 64].

3.2.3 – Intensity measurements

In order to examine the relationship between the radiation intensity and the resulting photochromic effect, the samples were irradiated using seven different intensities. This was achieved using ThorLabs' *neutral-density (ND) filters*, i.e. filters that reduce the intensity of all wavelengths equally. An ND filter is characterized by its absorbance (also known as optical density), which specifies the optical power transmittance:

$$d(\lambda) \equiv log\left(\frac{P(\lambda)}{P_T(\lambda)}\right) = log\left(\frac{1}{T(\lambda)}\right) \quad [-] \quad (3.1)$$

where d is the optical density, P is incident power, P_T is transmitted power and T is the transmittance at wavelength λ[69]. The ND filters were mounted as depicted in *Figure 3.6*. During photodarkening, only the fixed filter was applied. During bleaching, the combined optical density of the fixed and the rotatable filter was made as close to *d = 3.0* as possible.

Figure 3.6: Setup for intensity experiments[63, 64, 70].

In this project, the spectrometers are only able to measure the radiative intensity at each wavelength in arbitrary units (a.u.), that is, counts per arbitrary time interval. Thus, the actual power (J/s) of each wavelength must be calculated by *recording the total power* incident on the sample (using a separate power meter), and then *distributing this* according to the normalized intensity vs. wavelength spectrum:

$$P(\lambda) = I_{norm}(\lambda) * P_{tot} \quad [\mathrm{W}] \quad (3.2)$$

where P is the incident power of wavelength λ, I_{norm} is the normalized intensity of wavelength λ, and P_{tot} is the total power of all wavelengths combined. The power meter applied in this project – a ThorLabs power meter based on a thermal sensor – utilizes the thermoelectric effect observed in a conductor irradiated by the given light[71, 72].

3.2.4 – Wavelength measurements

To investigate how the photochromic effect of YH_x:O responds to different wavelengths, the samples were irradiated with light of various colours. This was achieved using ThorLabs' *longpass filters*, i.e. filters that only transmit longwave radiation above their so-called *cut-on wavelengths* (λ_{co}). One such longpass filter is depicted in *Figure 3.7*, along with its transmission spectrum.

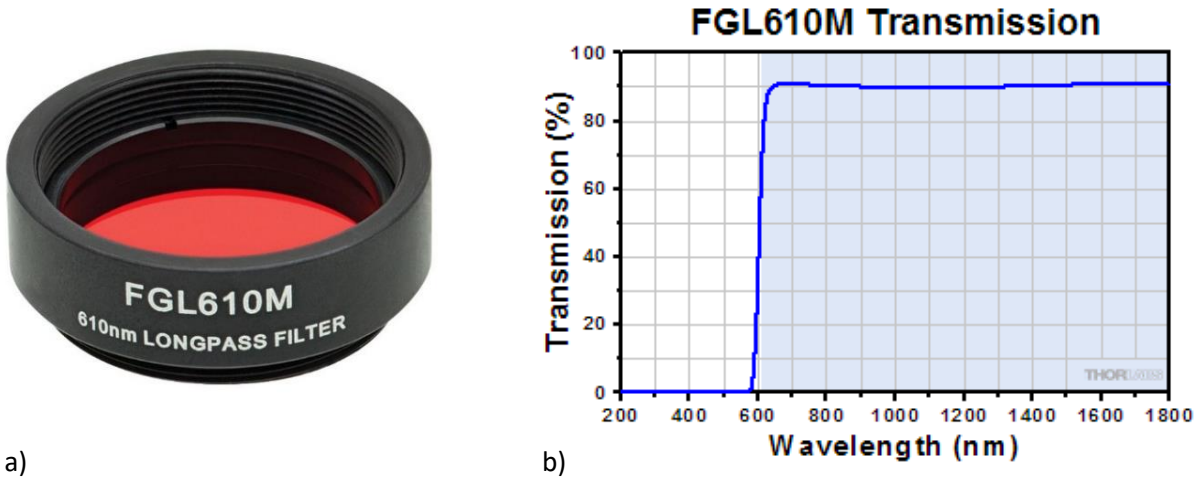

Figure 3.7: *a)* Longpass filter with a cut-on wavelength of λ_{co} = *610 nm*, and *b)* the transmission spectrum of the same filter[73].

The longpass filters were mounted according to *Figure 3.8*. No filter was applied during the photodarkening; the bleaching was initiated by rotating the longpass filter into position.

Note that the wavelength interval over which the transmission was averaged was chosen in each case according to the cut-on wavelength of the filter (in order to exclude the darkened wavelengths).

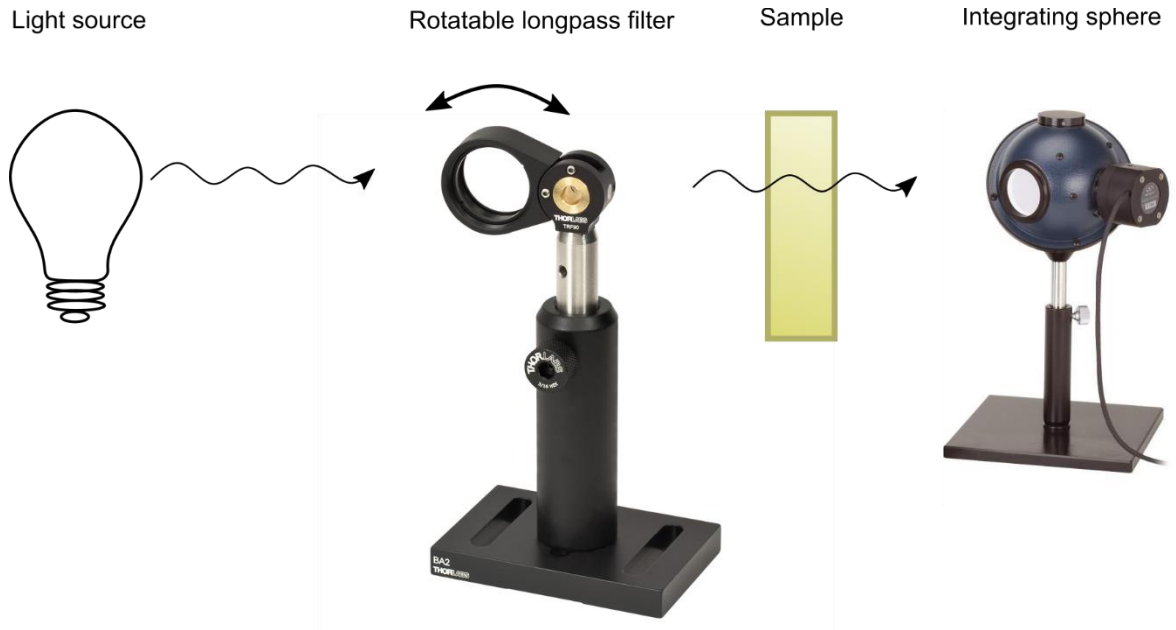

Figure 3.8: Setup for wavelength experiments[63, 64].

3.3 – Data processing and analysis

3.3.1 – Absorption

Quantitatively, there are several ways to express the process of absorption; This report relies on *absorptance, absorbance* and *absorption coefficient*. Absorptance is defined as the fraction of irradiated power transferred to the material, and can be calculated as

$$A(\lambda) = 1 - T(\lambda) + R(\lambda) \quad [-] \quad (3.3)$$

where A is absorptance, T is transmittance and R is reflectance at wavelength λ[69]. Similarly, the absorbance specifies the optical power transmittance when reflectance is assumed negligible (*Equation 3.1*). The absorption coefficient denotes the fraction of incident radiation absorbed per unit thickness of a material:

$$\alpha \equiv \frac{1}{x}\, ln\left(\frac{1 - R(\lambda)}{T(\lambda)}\right) \quad [cm^{-1}] \quad (3.4)$$

with α being the absorption coefficient, T the transmittance, R the reflectance and x the pathlength travelled by light through the material[69]. The latter corresponds to the sample thickness described in *Section 3.2.1*.

3.3.2 – Band gap: Tauc plot

The band gap of a semiconductor may be determined by a so-called Tauc plot. A Tauc plot utilizes the fact that a material's optical absorbance strength depends on the difference between its band gap energy and the photon energy:

$$(\alpha h\nu)^m = \beta\left(h\nu - E_g\right) \quad \left[\left(\frac{J}{cm}\right)^m\right] \quad (3.5)$$

where α is the absorption coefficient, $h\nu$ is the photon energy, E_g is the band gap energy, and β is a proportionality constant known as the band tailing parameter[74]. The exponent denotes the nature of the electronic transition,

- for direct allowed transitions: *m = 2,*
- for direct forbidden transitions: *m = 2/3,*
- for indirect allowed transitions: *m = 1/2*,
- for indirect forbidden transitions: *m = 1/3*.

Because the allowed transitions typically dominate an absorption process, the assumption in this project is that *m = 2* for direct transitions and *m = ½* for indirect transitions.

Plotting optical absorbance data $(\alpha h\nu)^m$ vs. energy of the incident radiation $(h\nu)$ will then produce a distinct linear region; extrapolating this region to the x-axis will yield the band gap of the material.

Note that in the case of very thin films, one would have to account for the reflection from the thin film-substrate interface.

3.3.3 – Reaction rates, rate constants and characteristic times

Instantaneous reaction rates are obtained graphically, as the derivative of the photodarkening:

$$r(t) = \frac{d}{dt}\Delta T(t) \quad \left[\frac{\%\ points}{s}\right] \quad (3.6)$$

in which r is the reaction rate and ΔT is the photodarkening at time t.

The characteristic time τ – alternatively, the rate constant k – of a reaction can be estimated by fitting a mono-exponential curve (*Equation 2.12*) to the observed transmission vs. time data. In this project, curve fitting is performed in the OriginPro 8 software, using the Levenberg-Marquardt algorithm. The fittings were mostly performed on raw data; however, the bleaching curves were sometimes shifted vertically to correct for obvious calibration discrepancies between the photodarkening and bleaching measurements.

3.3.4 – Activation energy: Arrhenius plot

The activation energy is calculated from Arrhenius' equation (*Equation 2.4*), using rate constants obtained at different temperatures. Taking the natural logarithm and rearranging this equation will yield a linear equation:

$$ln(k_t) = \frac{-E_a}{R}\left(\frac{1}{T}\right) + l\,n(A) \quad [-] \quad (3.7)$$

in which k_t is the thermal rate constant, E_a is the activation energy, R is the universal gas constant, T is the absolute temperature, and A is the frequency factor. Thus, when the rate constant behaves according to the Arrhenius equation, a plot of $ln(k)$ vs. T^{-1} should produce a straight line, whose slope equals ($-E_a/R$). Using the slope to calculate the activation energy E_a should then be straightforward.

3.3.5 – Number of photons

The energy E of a single photon is

$$E(\lambda) = \frac{hc}{\lambda} \quad [J] \quad (3.8)$$

where h is Planck's constant, c is the speed of light and λ is the photon wavelength. Combining *Equation 3.5* with the calculated power of each wavelength (*Equation 3.2*) allows for the estimation of the total number of photons incident on the sample during illumination:

$$N = \sum_{\lambda=\lambda_{min}}^{\lambda_{max}} \frac{P(\lambda)}{E(\lambda)} * t \quad [photons] \quad (3.9)$$

where N is the number of photons, P is the recorded incident power, E is the calculated photon energy and t is the illumination time. When investigating photons carrying energies higher than the band gap energy, the band gap wavelength λ_g is inserted as λ_{max}

4. Results and discussion

This chapter consists of the six following sections:

1. Initial sample properties
2. Photochromism at standard laboratory conditions
3. The effect of temperature
4. The effect of intensity
5. The effect of wavelength
6. Reaction mechanisms.

4.1 – Initial sample properties

After sputtering, the samples were stored in air in complete darkness for three weeks. Before any photodarkening experiments were conducted, the initial transmittance and reflectance spectra, as well as sample thickness, were obtained.

The thickness of *Sample 1.0* was measured to be $x_{S1.0} = 950$ nm. Because of uneven sputtering and a poorly controlled oxidation processes, the thickness is experienced to vary $\lesssim 10$ % across each sample, and slightly more between different samples. The samples are assumed to be similar for the experiments conducted in this project; nevertheless, a discussion regarding the potential consequences of sample differences is given in *Appendix A1*.

A collection of the transmittance and reflectance spectra for all samples are reserved for *Appendix A1*, and exemplified by the spectra of *Sample 1.0* in *Figure 4.1* (next page). The absorption edge of *Sample 1.0* is located at about 495 nm, corresponding to electron energies of about 2.5 eV. The transmittance is ~85-95 % at photon energies below the absorption edge (i.e. visible light), and ~0 % above the edge.

The spectra of *Sample 1.0* are similar to previous findings for YH_x:O, albeit with a slightly higher reflectance[28]. This discrepancy is probably a systematic error due either to inaccurate calibration, or to the assumption that no radiation is reflected at the film/substrate or the substrate/air interfaces. Previous attempts to correct for the film/substrate reflection have not been successful.

The oscillations present in the transmittance and reflectance spectra are caused by interference effects. A small offset between the interference patterns is to be expected, because of thickness variations, reflection at the film/substrate interfaces, the instability of the light source, and because the applied spectrophotometer was unable to measure the transmittance and reflectance simultaneously. However, the offset between the interference patterns of *Sample 1.0* is an acceptable 1-2 nm.

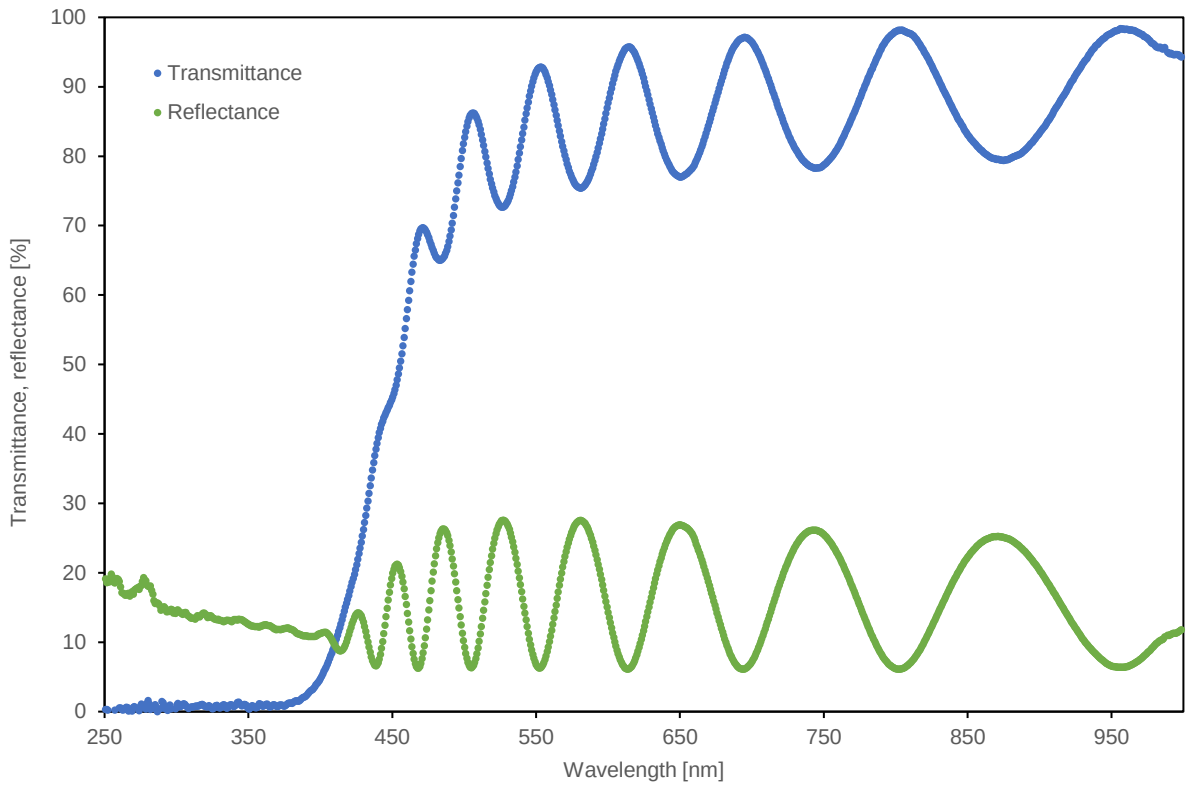

Figure 4.1: The transmittance, reflectance and absorbance spectra of *Sample 1.0*, recorded before any photodarkening experiments.

Indirect and direct optical band gaps of *Sample 1.0* were calculated by Tauc plots, as illustrated in *Figure A1.4* in *Appendix A1*. This yielded the following bandgap energies:

$$E_g = 2.5\ eV;\ \ Indirect\ transitions$$
$$E_g = 3.0\ eV;\ \ Direct\ transitions$$

corresponding to the wavelengths

$$\lambda_g = 496\ nm;\ \ Indirect\ transitions$$
$$\lambda_g = 413\ nm;\ \ Direct\ transitions$$

which are in agreement with the band gaps calculated for YH_x and YH_x:O by *Mongstad et al.* in 2010 and *You et al.* in 2014[52, 54]. The difference between the calculated indirect bandgap (2.5 eV) and the generally accepted value (2.6 eV) can be explained by the inaccuracy of the optical measurements, and possibly different compositions. For the purpose of this project, this discrepancy is considered insignificant. Because the material in this case is a lot thicker than 200 nm, indirect transitions are expected to dominate.

4.2 – Photochromism at standard laboratory conditions

Because photochromic YH_x:O was discovered only recently, step one of every project is to ensure that the sputtering yielded the correct material with the correct photochromic properties. Hence, the photochromic effect of *Sample 1* was tested at "standard laboratory conditions" (temperature ≈ 21-22 ˚C, humidity ≈ 25-26 %, and illumination as provided by the light source). The result is illustrated in *Figure 4.2*.

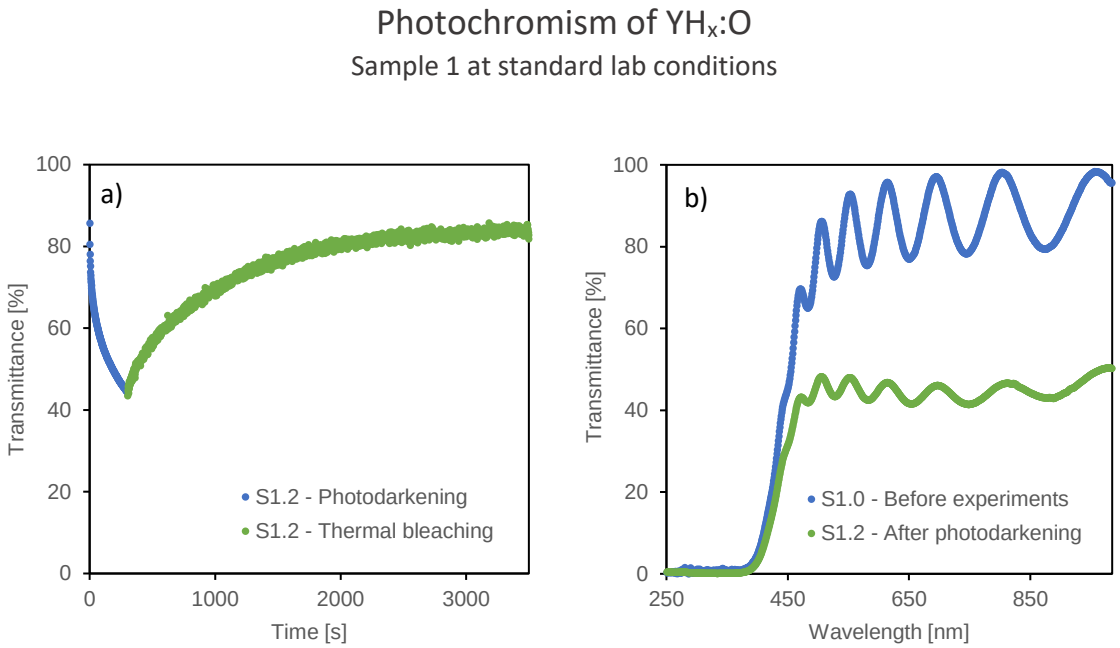

Figure 4.2: Time-resolved transmittance during photodarkening and bleaching (*a*), and transmittance spectra before and after photodarkening (*b*) at standard laboratory conditions. The transmittance was reduced by almost 50 % within 5 minutes.

Indeed, the sample experienced the strong photochromic effect characteristic of YH_x:O: After five minutes of exposure to UV/VIS radiation, the transmittance in the 500-900 nm interval was reduced from 86 % to 44 %. *Figure 4.2b* shows that the transmittance decreased at every observed wavelength greater than the band gap wavelength. The bleaching process was much slower than the photodarkening, with a full recovery being achieved only after more than one hour of darkness.

4.3 – The effect of temperature

The effect of temperature on the photochromic effect in YH_x:O was investigated in three steps:

1. Establishing a thermal effect
2. Heating the material during bleaching
3. Preheating the material prior to photodarkening and bleaching.

4.3.1 – Establishing a thermal effect

The first temperature experiment was performed to quickly investigate the relevance of a detailed experiment and the reliability of the setup. The procedure was to illuminate *Sample 6.5* at standard lab conditions, before simultaneously switching the light off and the heater on. *Figure 4.3* shows the first recording of thermal effects in photochromic YH_x:O. During illumination, the material experienced a temperature increase of only 2 ˚C due to the absorption of photons. This means that the material will not (by itself) risk overheating in times of great solar irradiation. However, it also means that photoinduced heating will not assist a thermal bleaching process.

After the illumination, the sample was heated with a blow dryer; first at a low power, then (accidentally) at a higher power. The transmittance curve clearly follows the temperature curve, though with a time lag of about fifty seconds. The maximum temperature achieved was 72 ˚C, at which the sample fully recovered to its initial transmittance (86 %). From this experiment, it can be concluded that increasing the temperature of YH_x:O greatly increases the rate of thermal bleaching. This called for a more systematic experiment with improved temperature control.

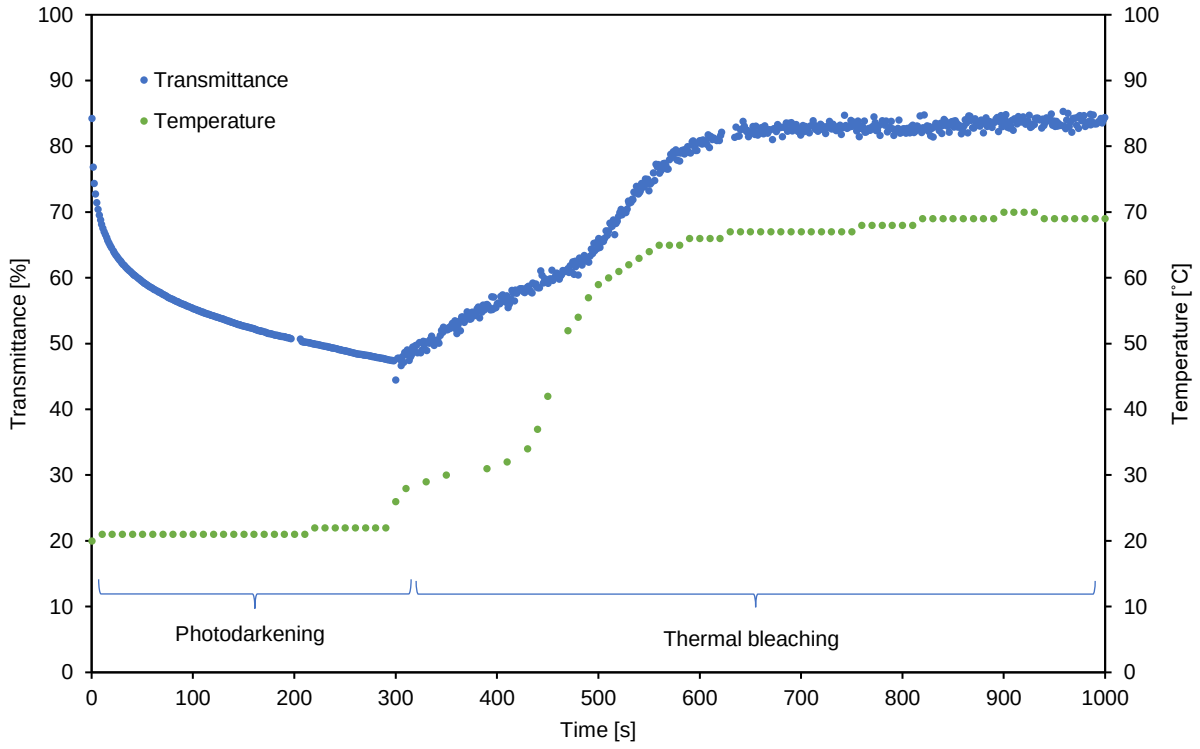

Figure 4.3: Thermal effects of photochromism in YH_x:O (*Sample 6.5*). The temperature increase due to illumination was 2 ˚C. After illumination, the sample was first heated at a low power, and then at a high power. The bleaching rate was clearly temperature dependent.

4.3.2 – Bleaching while heating

In the second experiment, all samples were illuminated for five minutes at standard lab conditions, before initiating the bleaching and heating simultaneously. The goal was to get a sense of the uncertainty in the measurements, and to isolate the bleaching process as much as possible.

The time-resolved transmittance and sample temperature during photodarkening are presented in *Figure 4.4.* During the illumination, the temperature increased by 1-3 ˚C. After five minutes of illumination, the average transmittance was 50 %, with a standard deviation of 2 percentage points. Note that the standard deviation is twice as large as before the experiment (*Table A1.1*). The degree of photodarkening correlates well with the assumed thickness variations of the samples, which are discussed in *Appendix A1*. Some of the samples also experience slightly different kinetics. Most of the deviation is likely a result of sample differences (e.g. thickness/composition), and human inaccuracy when uncovering the light source (which is done by rotating a dark filter away from the light beam).

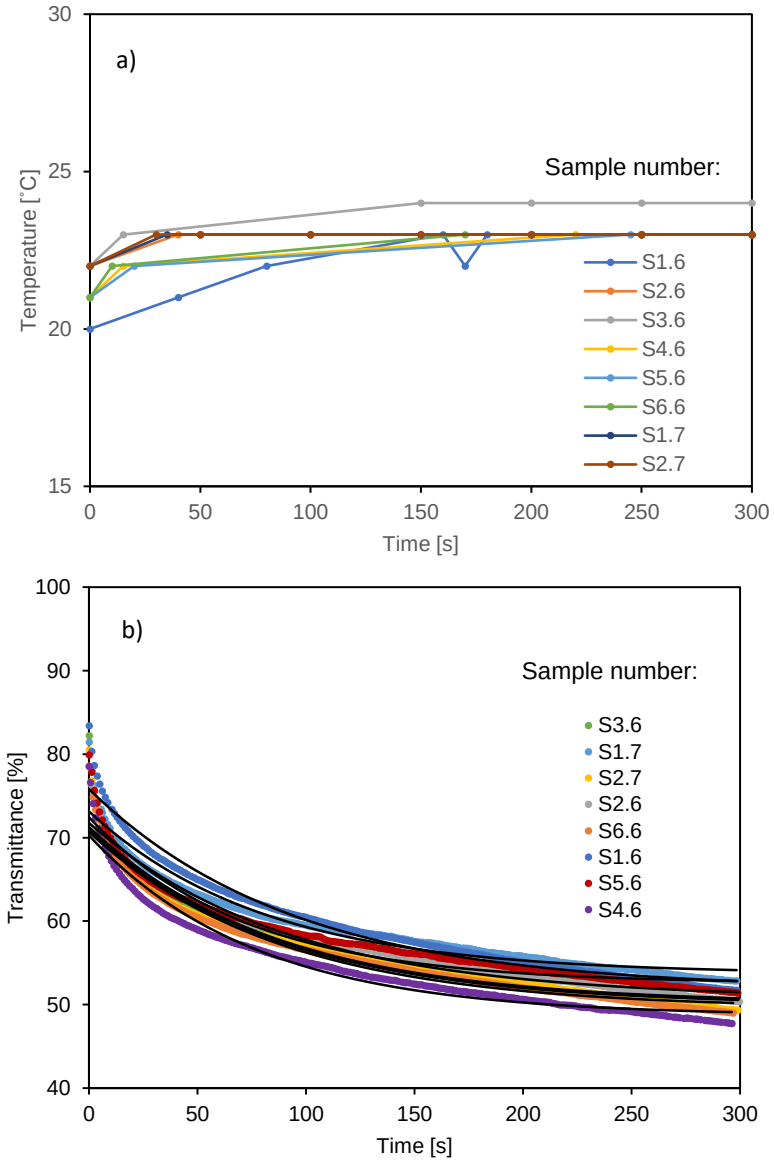

Figure 4.4: Transmittance during photodarkening at standard laboratory conditions.

The temperature recorded during the simultaneous heating and bleaching is plotted in *Figure 4.5a*. The temperature increased exponentially, consistent with Newton's law of heating. It took about 150 seconds to obtain semi-stable temperatures. The sudden drop in temperature of *Sample 4.6* was due to instabilities in the rather improvised setup. As it happened after most of the bleaching had already occurred, it does not affect the transmittance enough for the data to be discarded. From the error of the multimeter (±1 ˚C), thermocouple (±0.1 ˚C) and random fluctuations (±1 ˚C), the uncertainty of the temperature was estimated to $\sqrt{1^2 + 0.1^2 + 1^2} \approx 1$ ˚C.

The time-resolved transmittance is plotted in *Figure 4.5b,* together with the estimated mono-exponential curves. The results demonstrate a strong and systematic temperature-dependence of the thermal bleaching. Visually, the temperature dependence of the bleaching rate is apparent within 25-50 seconds. Because the temperatures in question is at or (relatively) close to room temperature, these results will not only be important during reaction analysis: They will also significantly affect possible applications of the material. The complete temperature and transmittance data sets (for $0 < t < 1000$ *s*) are available in *Figure A3.1* in *Appendix A3*.

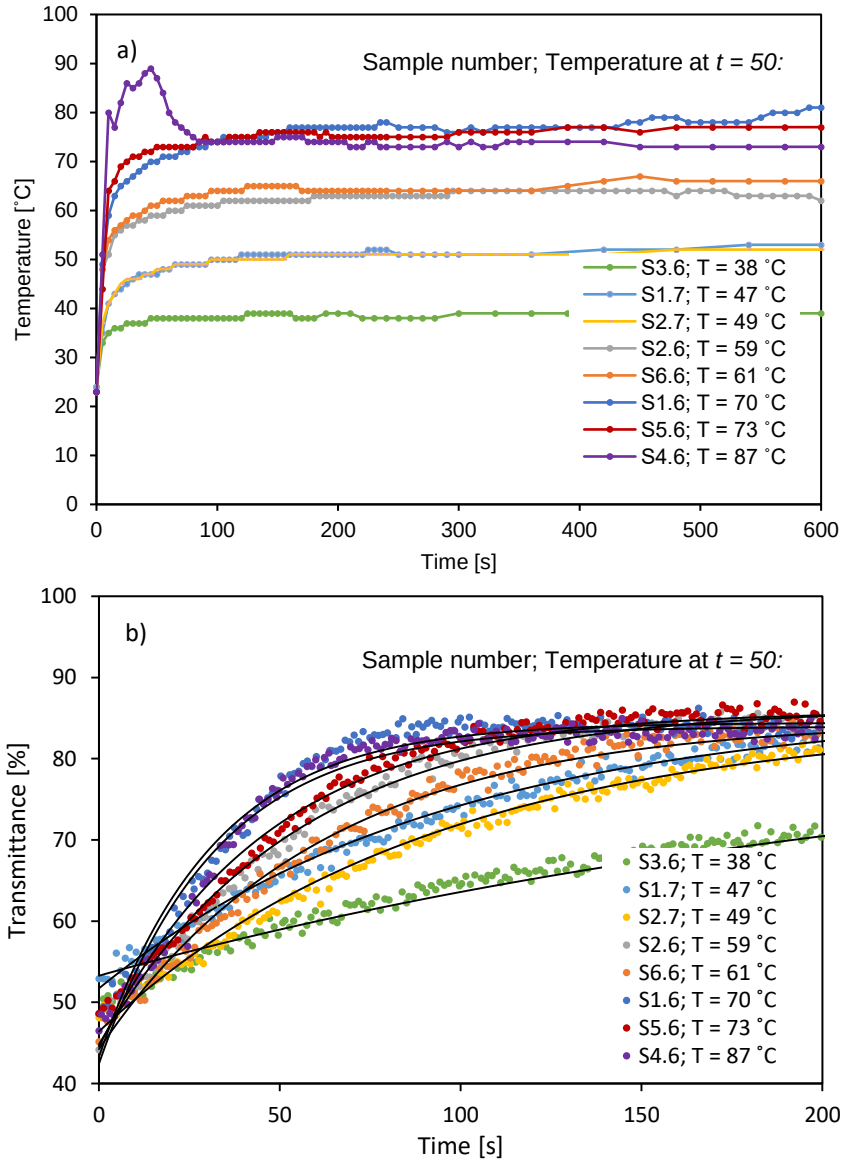

Figure 4.5: Sample temperature *(a)* and transmittance *(b)* during bleaching, when initiating heating and bleaching simultaneously. The temperatures in the insets were recorded at *t = 50 s.* The sudden temperature drop of *Sample 4.6* was due to instabilities in the setup.

The mono-exponential curves that were fitted to the transmittance data fit the data well, though the overestimation of *Sample 3.6* at low values of time *t* should be mentioned. In general, the accuracy of the estimated curves is expected to be within the accuracy of the experiments.

The final transmittance $T(t \rightarrow \infty)$ estimated by the fitted curves is independent of temperature: All samples fully recovered. Thus, this experiment does not indicate that increasing the temperature causes any immediate reduction of the bleaching cyclability. Dedicated life-time and cyclability analysis must, however, be conducted to ascertain this.

The time constants extracted from the exponential curves are plotted in *Figure 4.6,* as a function of the temperature at time $t = 50$ *s*. It is evident from the figure that the time constant decreases very quickly in the temperature interval 310-330 K (≈ 35-55 ˚C). The result was fitted with a mono-exponential function of the same form as the photodarkening. The fit is good, but not perfect – possibly because the temperature was not constant during the beginning of the bleaching process. More representative results are expected by preheating the samples.

Another source of error is the fact that the samples had slightly different transmittances when initiating the bleaching process. Two reasons for this have already been explained: The inherent sample properties and human error affecting the photodarkening process. Two additional reasons should be mentioned: The human error when initiating the bleaching process, and the error related to the sampling time of the spectrometers. The latter can cause the loss of important information in the beginning of the bleaching process, if the first transmittance measurement is performed several seconds after the bleaching was initiated. (In the case of the temperature experiments, the sampling time was approximately 1.2 s, within which the transmittance could increase several percentage points.) One way of reducing this problem, is to illuminate the samples until a predetermined transmittance is achieved (i.e. not necessarily for the same amount of time). Furthermore, automatically rotatable filters exist, but they are expensive compared to their expected advantage. The suggested improvements will be applied in the next experiment.

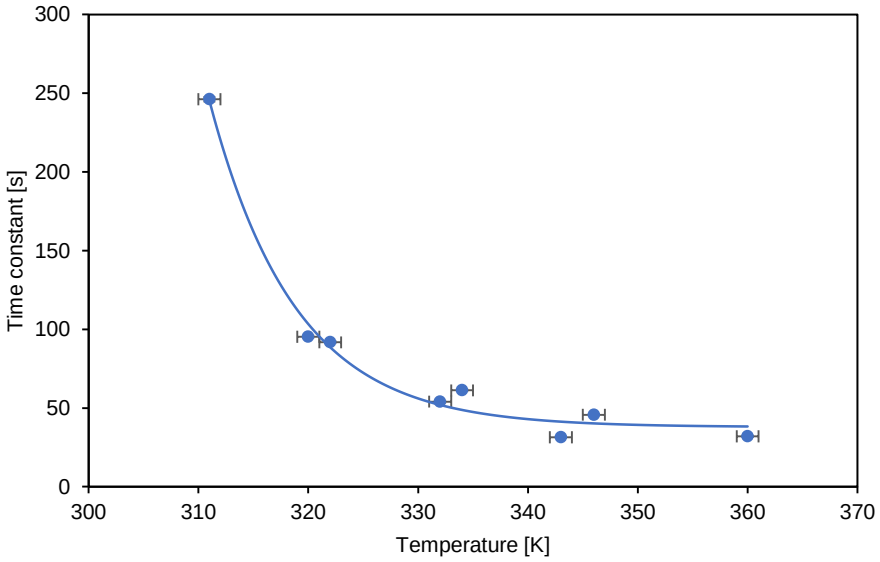

Figure 4.6: Estimated time constants of the bleaching process during which the samples were heated to different temperatures. Temperatures and time constants display an exponential relationship.

4.3.3 – Photochromism at different temperatures

In the third and final temperature experiment, the samples were preheated to different temperatures before initiating photodarkening to a predetermined transmittance of 50 %. The purpose was to obtain representative time constants for the photochromic darkening and bleaching of YH_x:O at different temperatures.

Figure 4.7 shows the time-resolved transmittance during photodarkening *(a)* and thermal bleaching *(b)* at six different temperatures. Clearly, the darkening rate decreases with temperature, while the opposite is the case for the bleaching rate. The first of these phenomena follows as a direct consequence of the latter, as bleaching also takes place during photodarkening.

This is the first proper study of thermal effects on the photochromism of YH_x:O. The systematic temperature dependence present in both the photodarkening and bleaching process indicates that the experiment was successful, and that further analysis will greatly improve the understanding of the observed photochromism.

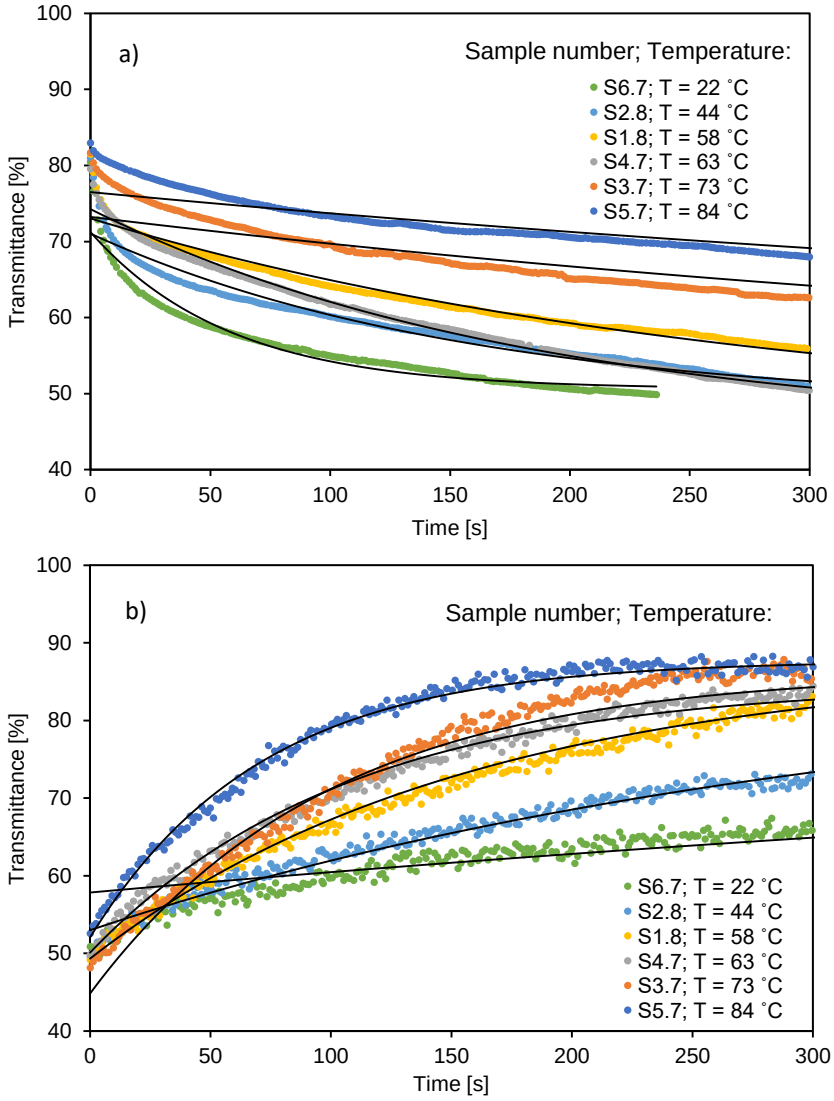

Figure 4.7: Transmittance during photodarkening *(a)* and thermal bleaching *(b)* at different temperatures; measured data and fitted exponential curves. Full dataset for *(a)* is in *Appendix A3*.

During both photodarkening and thermal bleaching, *Sample 4.7 (T = 44 ˚C)* stands out with a markedly irregular kinetic, compared to the other samples. The reason for this is not known, but it should be noted that the same sample experienced the strongest photodarkening out of all the samples in the previous experiment (*Figure 4.4b*). The photodarkening was then assumed related to sample thickness. It would be interesting to see this in relation to sample composition, as both the amount and rate of photodarkening have previously been linked to the oxygen content[28,54]. The possible effect of composition should be thoroughly investigated in a separate project.

Figure 4.7 also shows the exponential curves that were fitted to the data. During thermal bleaching, these curves provide a good fit. During photodarkening, the fit is good after about ten seconds, but less so at high darkening rates. This may suggest that the underlaying mechanism is more complicated than a mono-exponential decay. Nonetheless, the estimated equations are highly valuable when analysing the kinetics.

The estimated photostationary transmittance (PSST, after photodarkening) and final transmittance (after thermal bleaching) are given in *Table 4.1*. Regarding the final transmittance, all samples fully regenerated. Regarding the PSST, this is evidently higher at 84 ˚C than at 22 ˚C. In fact, the pre-determined transmittance of 50 % was not achieved for the hottest sample. In theory, this is as expected if the rate of thermal bleaching increases with temperature. In practice, this would mean that the possible degree of photodarkening is greater in cold climates than in hot climates, which may prove impractical. However, *Table 4.1* also shows that the samples reach approximately the same PSST for a large temperature span. Unless increasing the temperature also increases the probability of photodarkening, and this at some point gets offset by the probability of thermal bleaching, it seems no other explanation to this than the estimations being inaccurate. Upon closer visual inspection of *Figure 4.7a* and *Figure A3.3*, the fitted curves appear to over-estimate PPST slightly for temperatures 22-58 ˚C.

Table 4.1: Estimated photostationary transmittance (after photodarkening) and final transmittance (after thermal bleaching) at six different temperatures.

Sample number	Temperature [˚C]	Photostationary transmittance [%]	Final transmittance [%]
6.7	22 ± 2	49.6 ± 0.2	83.6 ± 0.2
2.8	44 ± 2	48.2 ± 0.4	86.5 ± 0.3
1.8	58 ± 2	46.2 ± 0.4	87.3 ± 0.4
4.7	63 ± 2	45.0 ± 0.4	84.8 ± 0.3
3.7	73 ± 2	49.9 ± 0.1	86.3 ± 0.5
5.7	84 ± 2	54.1 ± 0.1	87.7 ± 0.4

The time constants estimated for the darkening and bleaching of YH_x:O are plotted as a function of temperature in *Figure 4.8*. This figure shows that a temperature difference of 20 ˚C will have a big impact on the darkening and bleaching rate. Furthermore, lower temperatures favour high bleaching rates, while higher temperatures favour higher darkening rates. Note that the temperatures 20-60 ˚C are the most relevant for window applications.

A mono-exponential growth curve has been fitted to the darkening process, while a mono-exponential decay curve has been fitted to the bleaching process. The fit is good for both curves, with the exception of three outliers: *Sample 4.7 (T = 63 ˚C)* for both darkening and bleaching, and *Sample 3.7 (T = 73 ˚C)* for the darkening process only. While *Sample 4.7* has already been identified as irregular, the deviation of *Sample 3.7* is not known.

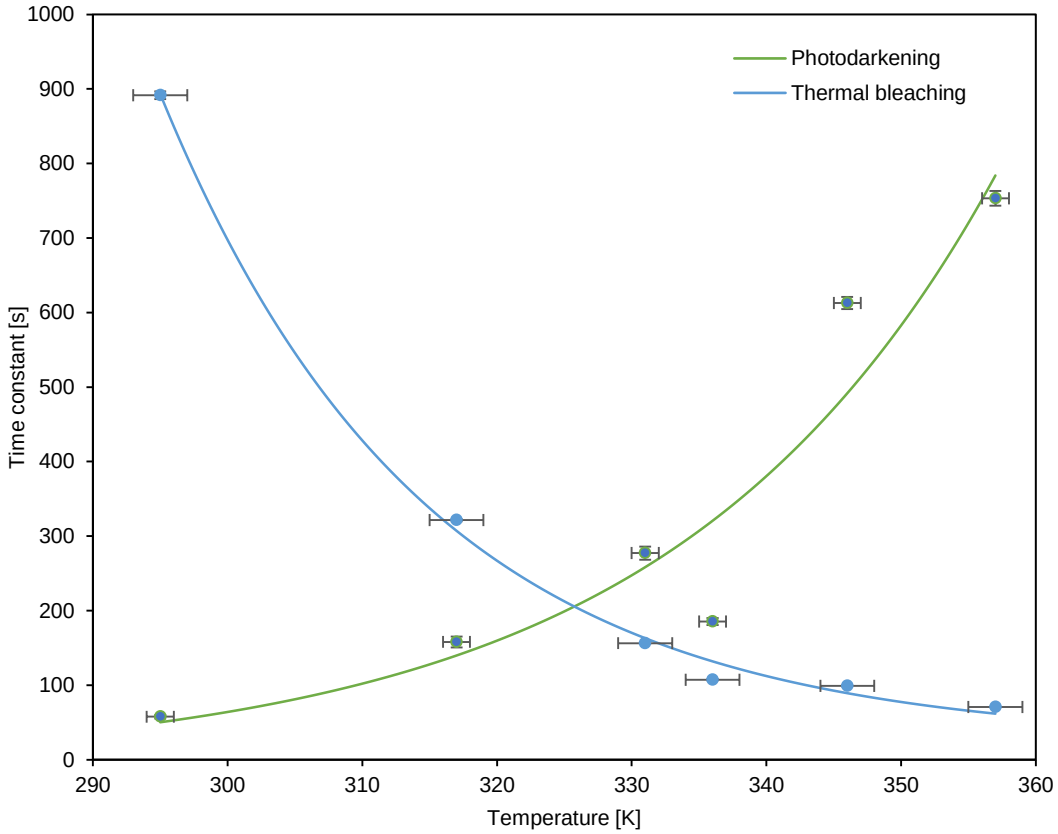

Figure 4.8: Time constants of the darkening and bleaching of YH_x:O at different temperatures. Mono-exponential curves have been fitted to the estimated values. The vertical error bars (which are almost too small to see) are the standard errors calculated during the curve fittings, while the horizontal error bars indicate the temperature uncertainty.

The temperatures were kept as constant as possible throughout the experiment. Temperature recordings, one of which is described in *Section 4.3.1,* revealed a photoinduced heating of 2 ˚C during photodarkening, followed by a maximum temperature fluctuation of ±2 ˚C during bleaching (see *Figure A3.2* in *Appendix A3* for all measurements). Reducing this uncertainty appears difficult without using more sophisticated transmission measurement with temperature control. An attempt to increase the stability by covering the equipment with a box was discarded.

Based on the reaction rate constants, which are the reciprocals of the time constants, the Arrhenius plots in *Figure 4.10* were calculated. The figure also includes the Arrhenius plot of the previous experiment 2. Recall from *Section 3.3.4 and 2.2.2* that Arrhenius plots visualises the relationship between the reaction rate and temperature, and provides important information regarding possible applications and reaction mechanisms. A steep slope indicates a strong temperature-dependency and, consequently, a high activation energy.

As *Figure 4.10* shows, the bleaching processes of the two experiments have similar slopes in the Arrhenius plot, suggesting that the experiments demonstrated similar temperature dependences. The vertical shift between the two experiments is a consequence of the samples of experiment 3 being preheated to stable temperatures, whereas the samples of experiment 2 were heated during the bleaching process. The latter involves a time delay between temperature and its influence on reaction rate, which results in lower time constants than those observed at the same temperatures in experiment 3. Regarding experiment 3, the same outliers are present in the Arrhenius plots as in the time constant plots. The absolute value of the darkening slope is similar to that of the bleaching slope, because the temperature-dependent bleaching occurs simultaneously as the temperature-independent photodarkening.

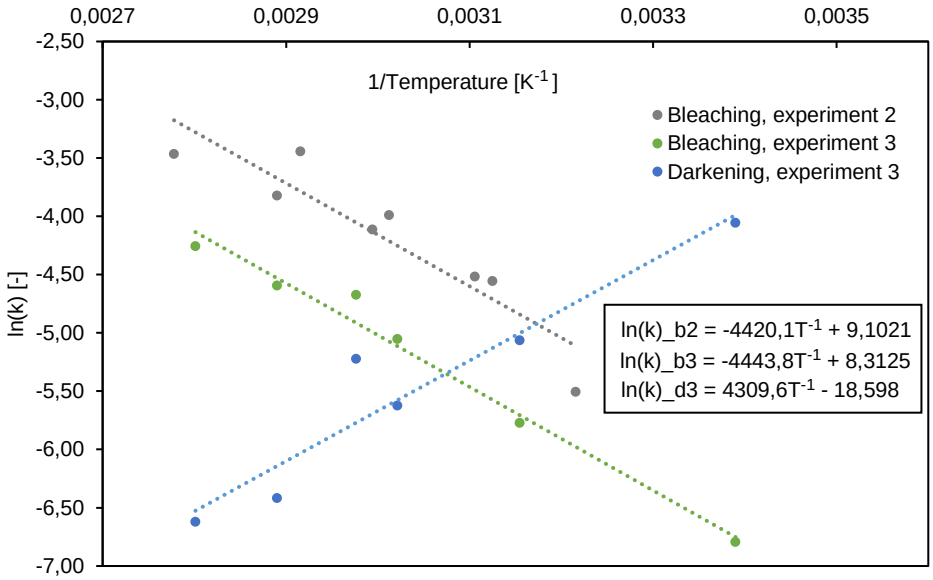

Figure 4.10: The Arrhenius plots of temperature experiments 2 and 3. The estimated linear curves of each dataset are given to the right in the figure.

From the Arrhenius plot of the bleaching process of experiment 3, the following activation energy was calculated:

$$E_a = 0.38\ eV$$

This rather low value reflects the fact that the bleaching process is temperature dependent, with room temperature being enough to initiate a reaction. As a comparison, the bond dissociation energies of yttrium-hydrogen (Y-H) or yttrium-oxygen (Y-O) bonds are 3.5 eV and 7.4 eV, respectively. Hence, the calculated activation energy is not enough to form or break Y-H or Y-O bonds, but it may be enough to distort them. A complete discussion regarding possible reaction mechanisms will be given in *Section 4.6*, after investigating the effect of incident intensity and wavelength.

From this experiment, it can be concluded that the photochromic effect of YH_x:O strongly depends on temperature. This is of great significance to future applications and reaction analysis.

4.4 – The effect of incident intensity

In this experiment, the samples were illuminated for five minutes by eight different intensities. To investigate the repeatability, which is essential to any commercial viability, the experiment was performed twice. The resulting time-resolved transmittance curves are plotted in *Figure 4.11*. The results show the photochromic effect of YH_x:O was successfully tuned by the use of neutral density filters, in a satisfyingly repeatable experiment. In both experiments, the transmission reduction was proportional to the incident intensity. This was expected, because increasing the radiative intensity (i.e. number of photons per second) increases the number of photoreactions possible within a time interval.

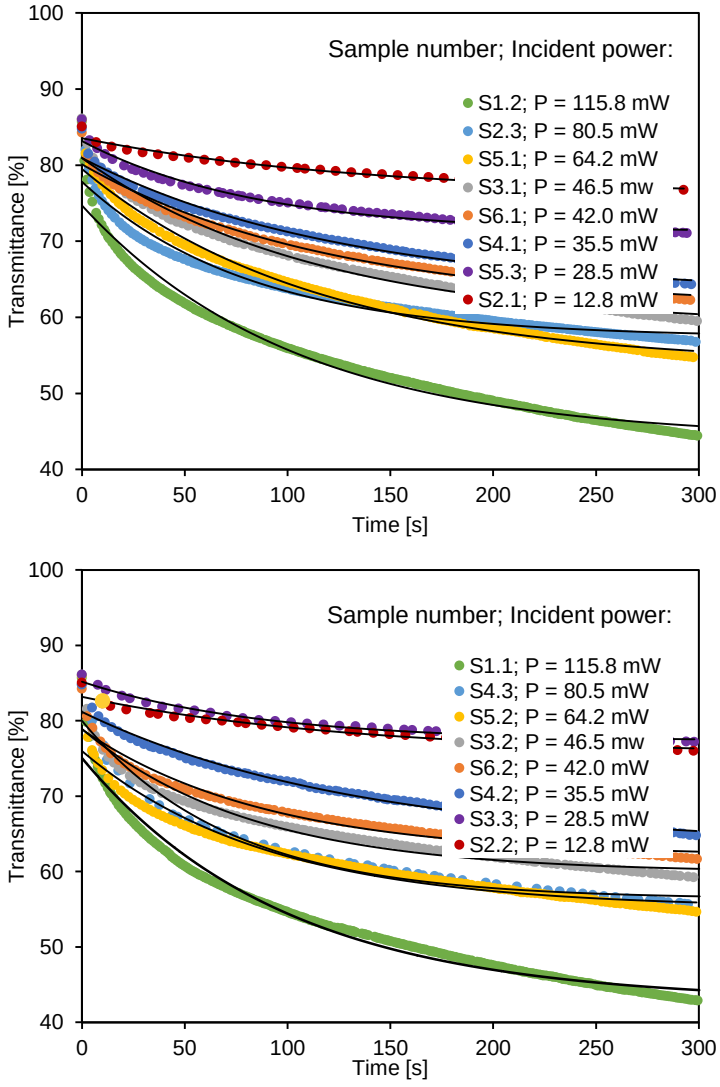

A conundrum to be observed from *Figure 4.11* is the irregular kinetics experienced in both experiments at 80.5 mW incident power. There is no obvious photophysical or photochemical explanation to why this particular intensity should affect the darkening rates as much as is observed. Different samples were used in the two cases, justifying the assumption that there might be something was wrong with the applied ND filter (optical density *d = 0.1*). All filters are investigated in *Appendix A2*, in which it is concluded that the applied filter transmitted 11.5 mW (14 %) less power than it ought to. This could explain a weakened photochromic effect, but presumably not the markedly different shape of the transmittance curve. Furthermore, the *d = 0.2* and *d = 0.3* filters also transmitted less than their ideal values, without this having any obvious effect on their kinetics. Also note that the spectra of all filters were as expected. Thus, the irregular kinetics at 80.5 mW remains unknown, and could be further investigated.

Figure 4.11: Time-resolved transmittance of samples irradiated by different intensities. The same experiment was performed twice: *a)* first experiment; *b)* repeated experiment. The measured data are plotted in colours, while the fitted mono-exponential curves are black.

The biggest difference between the two experiments, is observed at 28.5 mW. This discrepancy is assumed to be a one-off, because the observation of Experiment 2 clearly diverges from the trend. The difference may be explained by the combined uncertainty of *Sample 3.3* (28.5 mW, Experiment 2) and *Sample 2.2* (12.8 mW, Experiment 2).

The estimated time constants and photostationary transmittances (PSST) of both experiments are summarized in *Table 4.2*. The time constants generally increase with decreasing incident intensity. This trend could be expected to be even more obvious, because a higher photon flux would increase the rate of electron excitations and accompanying photoreactions. However, there's a rather high level of discrepancy in Experiment 2. The photostationary transmittances estimated for the two experiments show a high level of agreement and low standard errors. (The only obvious deviations are observed in the samples illuminated at 80.5 mW, which have already been discussed.)

Table 4.2: The estimated photostationary transmittances and time constants for the two identical intensity experiments. The standard errors were calculated by the curve fitting software.

Incident power [mW]	Photostationary transmittance [%]		Time constant [s]	
	Experiment 1	Experiment 2	Experiment 1	Experiment 2
115.8	44.0 ± 0.3	42.3 ± 0.3	104 ± 3	98 ± 3
80.5	57.4 ± 0.2	55.8 ± 0.3	82 ± 3	72 ± 4
64.2	53.7 ± 0.3	54.4 ± 0.3	115 ± 4	90 ± 4
46.5	58.8 ± 0.3	59.3 ± 0.3	115 ± 5	82 ± 4
42.0	61.3 ± 0.3	61.5 ± 0.2	122 ± 5	90 ± 4
35.5	63.2 ± 0.3	62.8 ± 0.3	126 ± 6	134 ± 6
28.5	71.1 ± 0.2	77.1 ± 0.1	85 ± 4	88 ± 5
12.8	76.0 ± 0.3	74.1 ± 0.4	139 ± 14	133 ± 16

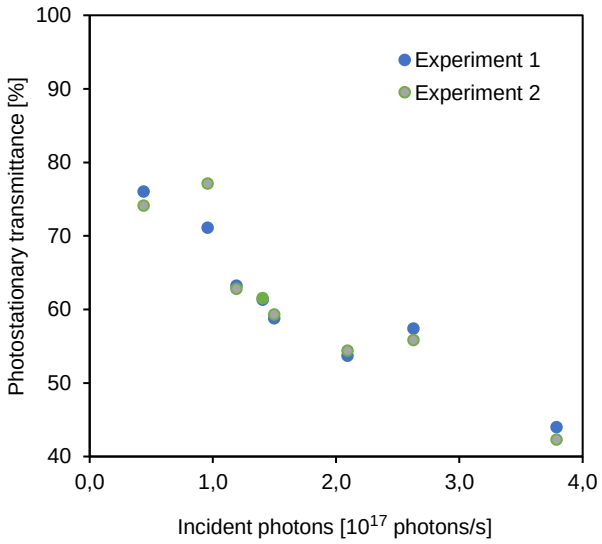

Plotting the photostationary transmittance as a function of the number of photons per second, demonstrates a linear relationship between the two (*Figure 4.12*). This indicates that simple one-to-one excitation processes may be responsible for the photodarkening of YH_x:O, as opposed to e.g. chain reactions. The intensity-dependency is highly beneficial in practice, as it means that e.g. windows and sunglasses will progressively filter out excess sunlight.

Figure 4.12: Estimated photostationary transmittance as a function of the number of incident photons, for the two identical intensity experiments.

After the illumination, thermal bleaching was initiated by covering the light source with two neutral density filters with a combined optical density as close to *d = 3.0* as possible. When having to choose between optical densities higher or lower than 3.0, a key element was to ensure enough illumination for the sensor to extract useful data (while still achieving proper bleaching). The unavoidable differences between the applied optical densities should be treated as a source of inaccuracy; however, the calculated transmission was only 0.1 mW and 0.7 mW for the lowest (*d = 2.2*) and highest (*d = 3.1*) optical densities, respectively.

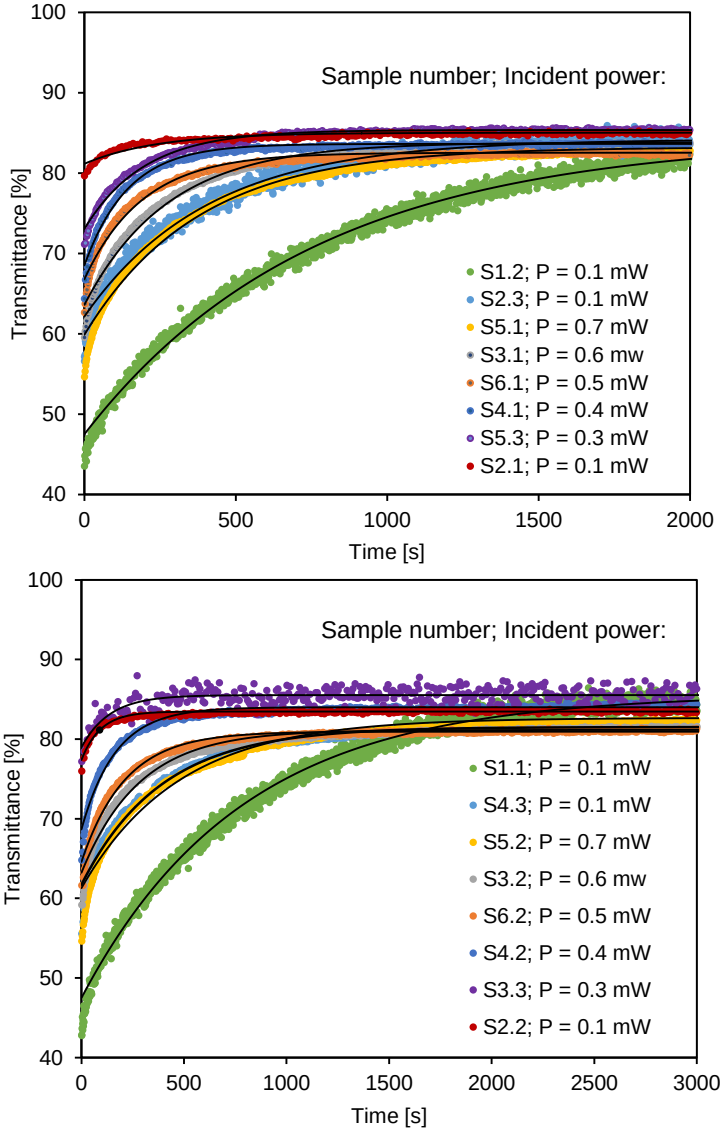

The time-resolved transmittance of the bleaching process is plotted in *Figure 4.13*. Once again, the plots demonstrate a high level of repeatability of the experiment. Furthermore, the plots indicate that the reaction rate is higher at lower transmittances. This is as expected from the assumption that all photodarkened states have the same reaction probability. It is interesting from an application point-of-view, as it means that moments of greater irradiation are followed by quick back-reactions. It is worth noting that the samples that have been heavily illuminated appear to not fully regenerate (i.e. slightly stronger memory-effect); this can also be explained by statistics.

Figure 4.13: Time-resolved transmittance of bleaching from different transmittances. Neutral density filters of slightly different optical densities were applied to initiate the bleaching process. *a)* first experiment, *b)* repeated experiment.

The estimated final transmittances and time constants of both executions are summarized in *Table 4.3*. Note the very small standard error estimated for the final transmittances (this does not include experimental errors). Regarding the final transmittances themselves, it is possible that the power incident on the samples during bleaching – although very low – prevented complete regeneration. If this is the case, it means that the applied method involves a noticeable error caused by the probe light. A possible solution is to increase the filter strength, but this would also increase the noise significantly. A better solution would probably be to increase the intensity, and use this (together with the photodarkening experiment) to model the transmittance as a function of incident intensity. This way, one could correct for the unwanted low-intensity probe light in coming experiments. *Table 4.3*: The estimated final transmittances and time constants for the two identical bleaching experiments. The standard errors were calculated by the curve fitting software.

Incident power [mW]	Final transmittance [%]		Time constant [s]	
	Experiment 1	Experiment 2	Experiment 1	Experiment 2
0.1	84.4 ± 0.1	85.6 ± 0.1	757 ± 3	779 ± 3
0.1	80.4 ± 0.1	81.5 ± 0.1	394 ± 3	387 ± 4
0.7	83.2 ± 0.1	82.7 ± 0.1	375 ± 2	475 ± 2
0.6	83.8 ± 0.1	81.2 ± 0.1	279 ± 2	283 ± 2
0.5	82.5 ± 0.1	80.9 ± 0.1	194 ± 2	213 ± 1
0.4	83.6 ± 0.1	84.0 ± 0.1	144 ± 1	167 ± 2
0.3	85.4 ± 0.1	85.5 ± 0.1	197 ± 1	138 ± 14
0.1	85.0 ± 0.1	83.5 ± 0.1	240 ± 11	93 ± 3

Plotting the time constants as a function of the transmittance before bleaching (i.e. photostationary transmittance, *Table 4.2*), demonstrates a weakly exponential trend (*Figure 4.14*).

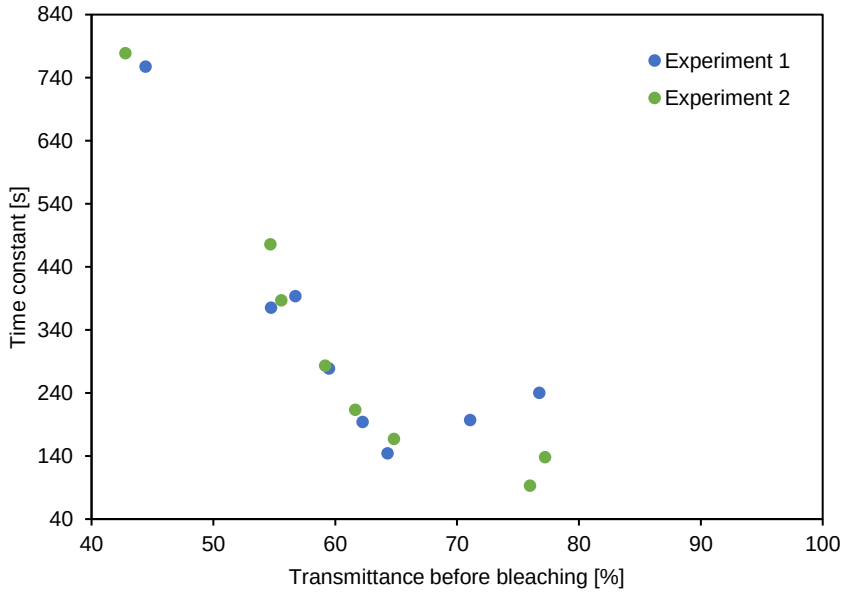

Figure 4.14: Estimated time constants during bleaching as a function of the transmittance before the bleaching. The same experiment was executed twice.

4.5 - The effect of incident wavelengths

To investigate how different wavelengths influence the photochromic effect, filters of different colours (cut-on filters) were used to manipulate the incident light. The optical properties of these filters are discussed in *Appendix A2.* Generally, the radiation transmitted by the filters will not offset thermal bleaching, meaning that the samples must be photodarkened by stronger radiation before applying the filters. Thus, the samples were illuminated at standard lab conditions for five minutes, before initiating bleaching with differently coloured filters. The time-resolved transmittance curves of the photodarkening process are given in *Appendix A4, Figure A4.1*.

Figure 4.15 shows the average transmittance in the 500-900 nm interval during thermal bleaching, when illuminating four different samples with differently coloured light. The equilibrium transmittance is clearly higher at higher cut-on wavelengths. However, the big pit-fall of this experiment is that increasing the cut-on wavelength also decreases the total intensity. When comparing *Figure 4.15* to *Figure 4.11* (intensity-dependence of photodarkening), it is clear that the differences observed between cut-on wavelengths 495, 550 and 610 nm could in fact be a result of different intensities. Similar results were obtained at higher cut-on wavelengths, as shown in *Figure A4.2* in *Appendix A4*. This theory is supported by plotting the time constants as a function of incident power (*Figure 4.16*, next page), which demonstrates an exponential relationship.

The big difference between cut-on wavelengths 400 and 495 nm, on the other hand, can possibly not be accounted for by the difference in total intensity. Moreover, when comparing the absolute values of each transmittance curve, it is evident that the incident powers that result in bleaching in the wavelength experiment (*Figure 4.15*) result in darkening in the intensity experiment (*Figure 4.11*). These observations could be caused by the increased photochromic response at photon energies higher than the band gap.

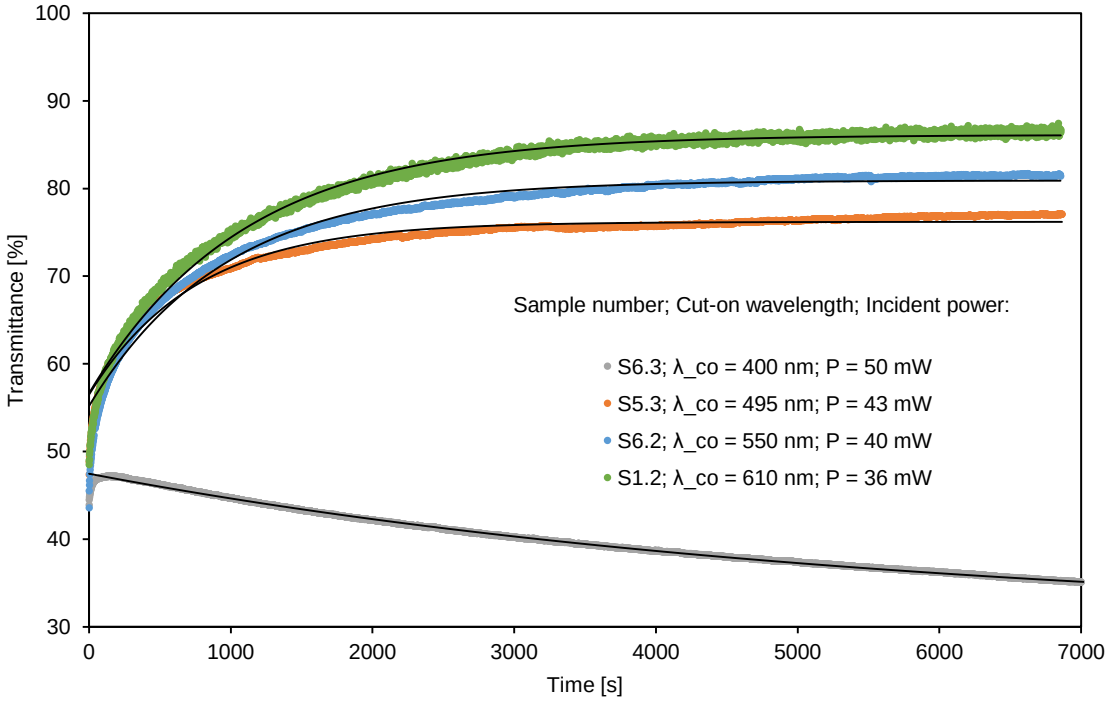

Figure 4.14: Bleaching when illuminated by different wavelengths; Average transmittance in 500-900 nm interval. When using the filter with a cut-on wavelength of 400 nm, *Sample 6.3* did not regenerate.

The fact that blue and UV light gives the strongest photodarkening, and that this corresponds to the band gap, is well known. Nonetheless, it is interesting to see that the change in the reaction probability is very abrupt: At the given intensities, photodarkening is not possible at photon energies below (approximately) the band gap. Hence, it is possible that the photochromism is more or less wavelength-independent a certain distance from the band gap, and that different levels of photodarkening observed here is mainly due to differences in intensities. It is, however, impossible to separate one parameter entirely from the other based on this experiment. Conclusive results can be obtained using lasers of equal intensity.

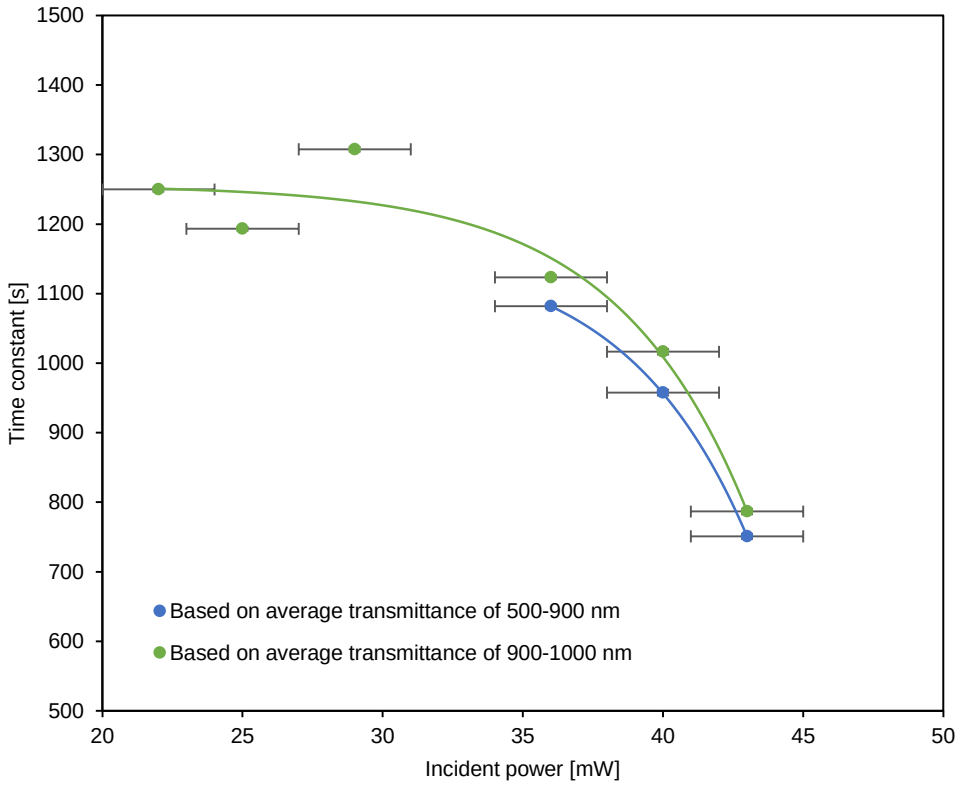

Figure 4.15: Time constants as a function of incident intensity for the bleaching process in which the samples were irradiated with different wavelengths. The time constants are based on the average transmittance in two different wavelength intervals (500-900 nm, and 900-1000 nm). Note that the 900-1000 nm interval is expected to be rather uncertain. The time constant obtained with the 400 nm cut-on filter is omitted, as it was 5623 s at 50 mW incident intensity.

4.6 – Reaction mechanisms

It has previously been suggested that the photochromic effect of YH_x:O is caused by the formation of small, metallic domains within the YH_x:O lattice upon illumination[48]. From the preceding discussions, it is evident that photons and heat play a key role in the reaction mechanisms. A possible explanation could be that the material experiences a form of photothermochromism, combining photoinduced electronic transitions with thermally induced atomic rearrangements.

In the suggested scenario, the photodarkening of YH_x:O is a result of photoexcitation of electrons from the oxygen (O) valence band to the yttrium (Y) conduction band. This would weaken the transparency-enhancing Y-O bond and thereby strengthen the Y-H bonds. The metallic domains are assumed to consist of such Y-H bonds. Increasing the radiative intensity implies an increased number of charge carriers, and hence more photoreactions. Shortly after the illumination, the abundance of Y-O bonds will result in high reaction rates. As the illumination time increases and the number of Y-O bonds decreases, the reduced probability of photoreactions will lower the reaction rates.

The bleaching could be the result of thermally induced tuning of the strength and length of the Y-O and Y-H bonds. If increasing the temperature were to strengthen the Y-H bond, the material would regain its initial transparency upon heating. The higher the temperature, the more mobile the hydrogen atoms will be, and hence the lower the transmission reduction upon illumination. At room temperature, the ion mobility does not play an important role.

Such a process would explain the observed lattice contraction and persistent photoconductivity upon illumination[26, 28]. It would also explain the accompanying changes in the local environment of the Y nucleus, and the appearance of mobile hydrogen[55]. The charge transfers have previously been predicted by theoretical simulations[53], but confirming this theory will require advanced synchrotron experiments.

6. Conclusions and further work

A reliable method for investigating thermal effects was developed through the work on this thesis. This method was used for photospectroscopic studies of the temperature- and irradiation-dependent changes in photodarkening and bleaching.

The investigation revealed that the photochromic effect in YH_x:O strongly depends on incident intensity and sample temperature. Temperature changes have a big impact on the photodarkening and thermal bleaching rates. Higher temperatures (above ~53 ˚C) favour higher photodarkening rates, while lower temperatures favour higher bleaching rates. The time constants demonstrated an exponential temperature-dependence of both the bleaching and photodarkening process.

The degree of photodarkening is directly proportional to the incident intensity, because increasing the radiative intensity increases the number of photoreactions possible within a time interval. Consequently, increasing radiative intensity will increase the photodarkening rate and decrease the bleaching rate. This experiment was found to be highly repeatable with regards to the estimated photostationary transmittances.

The effect of wavelength was more ambiguous, as some of the observations of this experiment may be attributed to the varying intensity. It seems plausible that an increased photodarkening was indeed observed at sub-bandgap wavelengths, but a decisive conclusion cannot be made without further investigations using a measurement setup tailored for this purpose.

A possible explanation to the above results could be that the photochromic effect in YH_x:O is driven by a combination of electronic transitions and rearrangement reactions. In the suggested scenario, the Y-O and Y-H bonds can be tuned by varying the photon flux or temperature. Consequently, YH_x:O may be classified as a photothermochromic material. Confirming the underlying photochemical reactions in this theory will require advanced synchrotron experiments.

Further work regarding the photochromic response of YH_x:O should include the following:

- Laser experiments to further investigate the effect of wavelength and intensity on the photochromic response. Lasers will allow the examination of distinct wavelengths separately, with the possibility to vary the intensity with neutral density filters. This will provide more accurate and conclusive results.
- More advanced temperature experiments, e.g. by improving the temperature control. It would also be interesting to investigate the effect of temperatures below room temperature. Whether or not the thermal bleaching ceases at some critical temperature will be of great importance to the performance of possible applications. Additionally, it will make it possible to separate the photoreaction from the thermal reaction, which is essential to a complete comprehension of the photochromic response.
- Investigations of the effect of composition/oxygen content. Previous research has indicated that the photoreaction rate might be greater at lower oxygen contents. If this (or the opposite) is the case, it could enable the tuning of optical properties according to given requirements and/or possibilities. An important sub-question will be the effect of sample thickness.
- Modelling of the photochromic response, as a function of parameters such as temperature, incident intensity, wavelength, reflectance, thickness and the number of darkened states. The model should separate the photoreaction from the thermal reaction, and enable the prediction of the time-resolved transmittance.

References

1. Thibaut Abergel, B. D., John Dulac (2017). *Towards a zero-emission, efficient, and resilient buildings and construction sector. Global Status Report 2017*: UN Environment and International Energy Agency.
2. IEA. (2013). *Transition to Sustainable Buildings - Strategies and Opportunities to 2050*. France: International Energy Agency.
3. Casini, M. (2015). *Smart windows for energy efficiency of buildings*, vol. 2.
4. Takaya, Y., Yasukawa, K., Kawasaki, T., Fujinaga, K., Ohta, J., Usui, Y., Nakamura, K., Kimura, J. I., Chang, Q., Hamada, M., et al. (2018). The tremendous potential of deep-sea mud as a source of rare-earth elements. *Sci Rep*, 8 (1): 5763. doi: 10.1038/s41598-018-23948-5.
5. Granqvist, C. G. (2003). Solar Energy Materials. *Advanced Materials*, 15 (21): 1789-1803. doi: 10.1002/adma.200300378.
6. Ye, H., Meng, X., Long, L. & Xu, B. (2013). The route to a perfect window. *Renewable Energy*, 55 (C): 448-455.
7. Ye, H., Meng, X. & Xu, B. (2012). Theoretical discussions of perfect window, ideal near infrared solar spectrum regulating window and current thermochromic window. *Energy and Buildings*, 49: 164-172. doi: https://doi.org/10.1016/j.enbuild.2012.02.011.
8. Martin-Palma, R. J. (2009). Spectrally selective coatings on glass: solar-control and low-emissivity coatings. *Journal of Nanophotonics*, 3. doi: Artn 030305 10.1117/1.3240868.
9. Tuchinda, C., Srivannaboon, S. & Lim, H. W. (2006). Photoprotection by window glass, automobile glass, and sunglasses. *Journal of the American Academy of Dermatology*, 54 (5): 845-854. doi: https://doi.org/10.1016/j.jaad.2005.11.1082.
10. ASHRA. (2009). *Handbook: Fundamentals*. Atlanta: American Society of Heating Refrigerating and Air-Conditioning Engineers.
11. Hutchings, P. B. a. M. G. (2010). *Chromic phenomena: Technological applications of colour chemistry*, vol. 2. Cambridge, UK: The Royal Society of Chemistry.
12. Wang, Z., Fan, W., He, Q., Wang, Y., Liang, X. & Cai, S. (2017). A simple and robust way towards reversible mechanochromism: Using liquid crystal elastomer as a mask. *Extreme Mechanics Letters*, 11: 42-48. doi: https://doi.org/10.1016/j.eml.2016.11.015.
13. Lampert, C. M. (2004). Chromogenic smart materials. *Materials Today*, 7 (3): 28-35. doi: Doi 10.1016/S1369-7021(04)00123-3.
14. La, M., Li, N., Sha, R., Bao, S. & Jin, P. (2018). Excellent photochromic properties of an oxygen-containing yttrium hydride coated with tungsten oxide (YHx:O/WO3). *Scripta Materialia*, 142: 36-40. doi: https://doi.org/10.1016/j.scriptamat.2017.08.020.
15. Wang, S., Liu, M., Kong, L., Long, Y., Jiang, X. & Yu, A. (2016). Recent progress in VO2 smart coatings: Strategies to improve the thermochromic properties. *Progress in Materials Science*, 81: 1-54. doi: https://doi.org/10.1016/j.pmatsci.2016.03.001.
16. Li, S. (2013). *VO2-based Thermochromic and Nanothermochromic Materials for Energy-Efficient Windows : Computational and Experimental Studies*. Doctoral thesis, comprehensive summary. Uppsala: Acta Universitatis Upsaliensis.
17. Dürr, H. (2003). General Introduction. In *Photochromism (Revised Edition)*, pp. 1-14. Amsterdam: Elsevier Science.
18. Pardo, R., Zayat, M. & Levy, D. (2011). Photochromic organic-inorganic hybrid materials. *Chem Soc Rev*, 40 (2): 672-87. doi: 10.1039/c0cs00065e.
19. Moretti, C., Tao, X., Koehl, L. & Koncar, V. (2016). Electrochromic textile displays for personal communication. In *Smart Textiles and their Applications*, pp. 539-568. Oxford: Woodhead Publishing.
20. Nakatani, K., Piard, J., Yu, P. & Métivier, R. (2016). Introduction: Organic Photochromic Molecules. In Tian, H. & Zhang, J. (eds) *Photochromic Materials*. Germany: Wiley-VCH.

21. Boggio-Pasqua, M. (2015). *Computational mechanistic photochemistry: The central role of conical intersections*: Université Toulouse III.
22. He, T. & Yao, J. (2006). *Photochromism in composite and hybrid materials based on transition-metal oxides and polyoxometalates*, vol. 51.
23. Vsevolodov, N. & Amiel, D. (1998). Photosensitive Materials for Use as Optical Memory. In Amiel, D. (ed.) *Biomolecular Electronics: An Introduction via Photosensitive Proteins*, pp. 131-175. Boston, MA: Birkhäuser Boston.
24. Kanu, S. S. & Binions, R. (2010). Thin films for solar control applications. *Proceedings of the Royal Society A: Mathematical, Physical and Engineering Science*, 466 (2113): 19-44. doi: 10.1098/rspa.2009.0259.
25. David Rips, D. K., Heidi W. Moore. (2007). Drivewear®, a New Lens Category for a Long-standing Need. *Refractive Eyecare* (January 2007).
26. Maehlen, J. P., Mongstad, T. T., You, C. C. & Karazhanov, S. (2013). Lattice contraction in photochromic yttrium hydride. *Journal of Alloys and Compounds*, 580: S119-S121. doi: 10.1016/j.jallcom.2013.03.151.
27. Gavrilyuk, A. I. (1999). Photochromism in WO3 thin films. *Electrochimica Acta*, 44 (18): 3027-3037. doi: https://doi.org/10.1016/S0013-4686(99)00017-1.
28. Mongstad, T., Platzer-Bjorkman, C., Maehlen, J. P., Mooij, L. P. A., Pivak, Y., Dam, B., Marstein, E. S., Hauback, B. C. & Karazhanov, S. Z. (2011). A new thin film photochromic material: Oxygen-containing yttrium hydride. *Solar Energy Materials and Solar Cells*, 95 (12): 3596-3599. doi: 10.1016/j.solmat.2011.08.018.
29. Plokker, M. P., Eijt, S. W. H., Naziris, F., Schut, H., Nafezarefi, F., Schreuders, H., Cornelius, S. & Dam, B. (2018). Electronic structure and vacancy formation in photochromic yttrium oxy-hydride thin films studied by positron annihilation. *Solar Energy Materials and Solar Cells*, 177: 97-105. doi: https://doi.org/10.1016/j.solmat.2017.03.011.
30. Mauser, H. & Gauglitz, G. (1998). *Photokinetics: Theoretical Fundamentals and Applications*: Elsevier Science.
31. Sánchez, J. M. O. (2009). *Excited state intramolecular proton transfer reactions coupled with non-adiabatic processes: Elextronic structure and quantum dynamical approaches*. Ph.D. Barcelona: Universitat Autònoma de Barcelona.
32. Ortiz-Sánchez, J. M., Gelabert, R., Moreno, M. & Lluch, J. M. (2008). Electronic-structure and quantum dynamical study of the photochromism of the aromatic Schiff base salicylideneaniline. *The Journal of Chemical Physics*, 129 (21): 214308. doi: 10.1063/1.3032215.
33. Sharon, M. (2016). Photoelectrochromism. In *An Introduction to the Physics and Electrochemistry of Semiconductors*. Canada: John Wiley & Sons, Scrivener Publishing LLC.
34. Daniels, F. (1959). Part I: General Considerations of Radiant Energy: Photokinetics11From the Department of Chemistry, University of Wisconsin, Madison, Wisconsin. *Journal of Investigative Dermatology*, 32 (2): 135-140. doi: https://doi.org/10.1038/jid.1959.28.
35. Butt, J. B. (2000). *Reaction Kinetics and Reaction Design*. 2 ed. New York: Marcel Dekker.
36. Delbaere, S., Vermeersch, G. & Micheau, J.-C. (2011). Quantitative analysis of the dynamic behaviour of photochromic systems. *Journal of Photochemistry and Photobiology C: Photochemistry Reviews*, 12 (2): 74-105. doi: https://doi.org/10.1016/j.jphotochemrev.2011.05.004.
37. Huiberts, J. N., Rector, J. H., Wijngaarden, R. J., Jetten, S., de Groot, D., Dam, B., Koeman, N. J., Griessen, R., Hjörvarsson, B., Olafsson, S., et al. (1996). Synthesis of yttriumtrihydride films for ex-situ measurements. *Journal of Alloys and Compounds*, 239 (2): 158-171. doi: https://doi.org/10.1016/0925-8388(96)02286-4.
38. Hoekstra, A. F. T., Roy, A. S., Rosenbaum, T. F., Griessen, R., Wijngaarden, R. J. & Koeman, N. J. (2001). Light-Induced Metal-Insulator Transition in a Switchable Mirror. *Physical Review Letters*, 86 (23): 5349-5352.

39. Ohmura, A., Machida, A., Watanuki, T., Aoki, K., Nakano, S. & Takemura, K. (2007). Photochromism in yttrium hydride. *Applied Physics Letters*, 91 (15): 151904. doi: 10.1063/1.2794755.
40. Wang, K., Hattrick-Simpers, J. R. & Bendersky, L. A. (2010). Phase transformation in an yttrium–hydrogen system studied by TEM. *Acta Materialia*, 58 (7): 2585-2597. doi: https://doi.org/10.1016/j.actamat.2009.12.045.
41. Vajda, P. (1995). Hydrogen in rare-earth metals, including RH(2+x) phases. In vol. 20 *Handbook on the Physics and Chemistry of Rare Earths*, pp. 207-291: Elsevier.
42. van Gelderen, P., Bobbert, P. A., Kelly, P. J. & Brocks, G. (2000). Parameter-free quasiparticle calculations for YH3. *Phys Rev Lett*, 85 (14): 2989-92. doi: 10.1103/PhysRevLett.85.2989.
43. Machida, A., Ohmura, A., Watanuki, T., Ikeda, T., Aoki, K., Nakano, S. & Takemura, K. (2006). X-ray diffraction investigation of the hexagonal–fcc structural transition in yttrium trihydride under hydrostatic pressure. *Solid State Communications*, 138 (9): 436-440. doi: https://doi.org/10.1016/j.ssc.2006.04.011.
44. Ohmura, A., Machida, A., Watanuki, T., Aoki, K., Nakano, S. & Takemura, K. (2006). Infrared spectroscopic study of the band-gap closure in YH3 at high pressure. *Physical Review B*, 73 (10): 104105.
45. Mongstad, T. T. (2012). *Thin-film metal hydrides for solar energy applications*. Ph.D. Oslo, Norway: University of Oslo.
46. Montero, J., Martinsen, F. A., Lelis, M., Karazhanov, S. Z., Hauback, B. C. & Marstein, E. S. (2018). Preparation of yttrium hydride-based photochromic films by reactive magnetron sputtering. *Solar Energy Materials and Solar Cells*, 177: 106-109. doi: 10.1016/j.solmat.2017.02.001.
47. Montero, J., Martinsen, F., Karazhanov, S., Hauback, B. & Marstein, E. (2016). *New insights into the photochromic mechanism in oxygen-containing yttrium hydride thin films: an optical perspective*.
48. Montero, J., Martinsen, F. A., Garcia-Tecedor, M., Karazhanov, S. Z., Maestre, D., Hauback, B. & Marstein, E. S. (2017). Photochromic mechanism in oxygen-containing yttrium hydride thin films: An optical perspective. *Physical Review B*, 95 (20). doi: 10.1103/PhysRevB.95.201301.
49. Musil, J., Baroch, P., Vlček, J., Nam, K. H. & Han, J. G. (2005). Reactive magnetron sputtering of thin films: present status and trends. *Thin Solid Films*, 475 (1): 208-218. doi: https://doi.org/10.1016/j.tsf.2004.07.041.
50. Moldarev, D., Primetzhofer, D., You, C. C., Karazhanov, S. Z., Montero, J., Martinsen, F., Mongstad, T., Marstein, E. S. & Wolff, M. (2018). Composition of photochromic oxygen-containing yttrium hydride films. *Solar Energy Materials and Solar Cells*, 177: 66-69. doi: 10.1016/j.solmat.2017.05.052.
51. Daou, J. N. & Vajda, P. (1992). Hydrogen ordering and metal-semiconductor transitions in the system YH(2+x). *Physical Review B*, 45 (19): 10907-10913.
52. Mongstad, T., Platzer-Bjorkman, C., Karazhanov, S. Z., Holt, A., Maehlen, J. P. & Hauback, B. C. (2011). Transparent yttrium hydride thin films prepared by reactive sputtering. *Journal of Alloys and Compounds*, 509: S812-S816. doi: 10.1016/j.jallcom.2010.12.032.
53. Pishtshev, A. & Karazhanov, S. Z. (2014). Role of oxygen in materials properties of yttrium trihydride. *Solid State Communications*, 194: 39-42. doi: 10.1016/j.ssc.2014.06.012.
54. You, C. C., Mongstad, T., Maehlen, J. P. & Karazhanov, S. (2014). Engineering of the band gap and optical properties of thin films of yttrium hydride. *Applied Physics Letters*, 105 (3). doi: Artn 031910 10.1063/1.4891175.
55. Chandran, C. V., Schreuders, H., Dam, B., Janssen, J. W. G., Bart, J., Kentgens, A. P. M. & van Bentum, P. J. M. (2014). Solid-State NMR Studies of the Photochromic Effects of Thin Films of Oxygen-Containing Yttrium Hydride. *The Journal of Physical Chemistry C*, 118 (40): 22935-22942. doi: 10.1021/jp507248c.
56. Xu, Y.-N., Gu, Z.-q. & Ching, W. Y. (1997). Electronic, structural, and optical properties of crystalline yttria. *Physical Review B*, 56 (23): 14993-15000.

57. Swann, S. (1988). Magnetron sputtering. *Physics in Technology*, 19 (2): 67.
58. Mattox, D. M. (2010). Vacuum Evaporation and Vacuum Deposition. In *Handbook of Physical Vapor Deposition (PVD) Processing*, pp. 195-235. Boston: William Andrew Publishing.
59. Granqvist, C. G. (2007). Transparent conductors as solar energy materials: A panoramic review. *Solar Energy Materials and Solar Cells*, 91 (17): 1529-1598. doi: https://doi.org/10.1016/j.solmat.2007.04.031.
60. Castro, C., Sanjines, R., Pulgarin, C., Osorio, P., Giraldo, S. A. & Kiwi, J. (2010). Structure–reactivity relations for DC-magnetron sputtered Cu-layers during E. coli inactivation in the dark and under light. *Journal of Photochemistry and Photobiology A: Chemistry*, 216 (2): 295-302. doi: https://doi.org/10.1016/j.jphotochem.2010.06.030.
61. Milano, P. d. (Unknown). *Sputtering System – AJA ATC Orion 8*. Available at: http://www.polifab.polimi.it/equipments/orion-8/ (accessed: 01.03.2018).
62. Pelleymounter, D. R., Christie, D. J. & Fries, B. D. (2015). *Pulsed DC Power for Magnetron Sputtering: Strategies for Maximizing Quality and Flexibility*.
63. ThorLabs. (Unknown). *90° Flip Mounts*. Available at: https://www.thorlabs.com/newgrouppage9.cfm?objectgroup_ID=1447&pn=trf90 (accessed: 01.03.2018).
64. Newport. (Unknown). *4-Port Integrating Sphere, 4 in., Barium Sulfate, Inc.0-Deg 1.5 in. Plug*. Available at: https://www.newport.com/p/819C-SF-4 (accessed: 01.03.2018).
65. OceanOptics. (Unknown). *NIRQuest512*. Available at: https://oceanoptics.com/product/nirquest512/ (accessed: 01.03.2018).
66. OceanOptics. (Unknown). *QE65000 Data Sheet*. New Zealand: Ocean Optics.
67. Unknown. (Unknown). *Lenovo IBM ThinkPad*. Available at: http://azteccomputersplus.com/?s=+Lenovo+IBM+ThinkPad&post_type=product (accessed: 01.03.2018).
68. OceanOptics. (Unknown). *STAGE-RTL-T, Reflection-Transmission Stage*. Available at: https://oceanoptics.com/product/stage-rtl-t/ (accessed: 01.03.2018).
69. Soares, J. (2014). *Introduction to Optical Characterization of Materials*.
70. ThorLabs. (Unknown). *Fixed Lens Mounts*. Available at: https://www.thorlabs.com/newgrouppage9.cfm?objectgroup_id=1433 (accessed: 01.03.2018).
71. ThorLabs. (Unknown). *PM16-425 - USB Power Meter, Thermal Sensor, 0.19 - 20 µm, 10 W Max* Available at: https://www.thorlabs.de/thorproduct.cfm?partnumber=PM16-425 (accessed: 01.03.2018).
72. ThorLabs. (Unknown). *Power Meter and Sensor Tutorial*. Available at: https://www.thorlabs.com/newgrouppage9.cfm?objectgroup_id=6188 (accessed: 01.03.2018).
73. ThorLabs. (Unknown). *Mounted Longpass Colored Glass Filters*. Available at: https://www.thorlabs.com/newgrouppage9.cfm?objectgroup_id=6395 (accessed: 01.03.2018).
74. Viezbicke, B. D., Patel, S., Davis, B. E. & Birnie, D. P. (2015). Evaluation of the Tauc method for optical absorption edge determination: ZnO thin films as a model system. *physica status solidi (b)*, 252 (8): 1700-1710. doi: doi:10.1002/pssb.201552007.

Appendices

A1. Initial sample properties 53
A2. Filter properties 55
A3. The effect of temperature. 57
A4. The effect of incident wavelength 59

A1. Initial sample properties

Figure A1.1 shows the transmittance and reflectance spectra of each sample, as measured before any photodarkening experiments were conducted. The interference fringe separation is clearly different for the different samples, indicating that the samples are not of the same thickness. Because the separation between the fringes are known to be bigger for thicker samples, the assumed order of the samples (from thick to thin) is *Sample 4, 6, 1, 5 or 2, 3*. The exact calculation of the differences is outside the scope of this project.

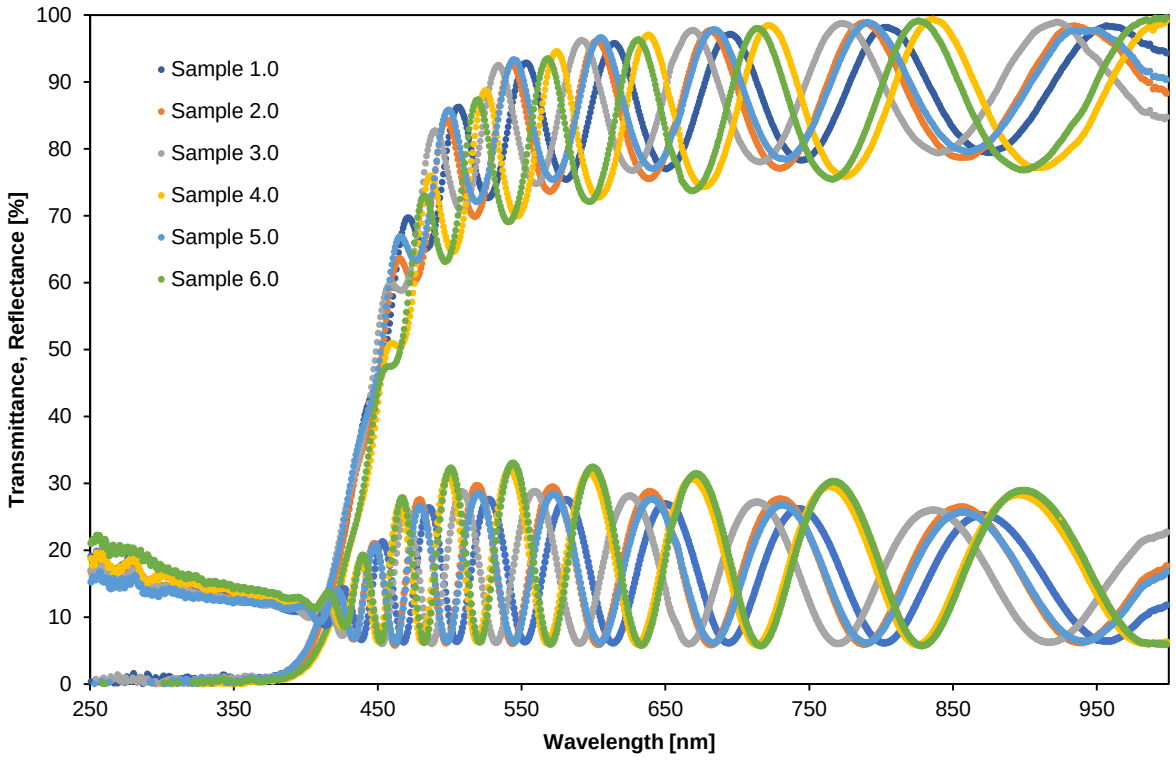

Figure A1.1: The initial transmittance spectra (top) and reflectance spectra (bottom) of all samples; as recorded three weeks after synthesis, before any photodarkening experiment was performed.

The average transmittance of the samples within the wavelength intervals 500-900 nm and 900-1000 nm are given in *Table A1.1*. In the 500-900 nm interval, the thinnest samples are also the most transparent (and vice versa). The low transmittance (and high reflectance) of *Sample 4 and 6* is also evident from *Figure A1.1.* The calculated transmittance in the interval 900-1000 nm is more uncertain, because it depends on the phase of the interference. It is included for the sake of the wavelength experiment, in which shorter wavelengths are sometimes excluded.

Table A1.1: Average transmittances in two different wavelength intervals.

Wavelength interval [nm]	Average transmittance [%]					
	Sample number					
	1.0	2.0	3.0	4.0	5.0	6.0
500-900	85,71	85,09	86,12	84,80	85,99	84,27
900-1000	94,00	94,36	92,67	86,82	94,52	89,21

Based on the transmittance and reflectance measurements, Tauc plots were calculated according to *Equation 3.5*. The Tauc plots for direct allowed and indirect allowed transitions are illustrated in *Figure A1.2*. Extrapolating the linear regions to the x-axis, yields the following band gaps:

$$E_g = 2.5\ eV;\ \ Indirect\ transitions$$
$$E_g = 3.0\ eV;\ \ Direct\ transitions$$

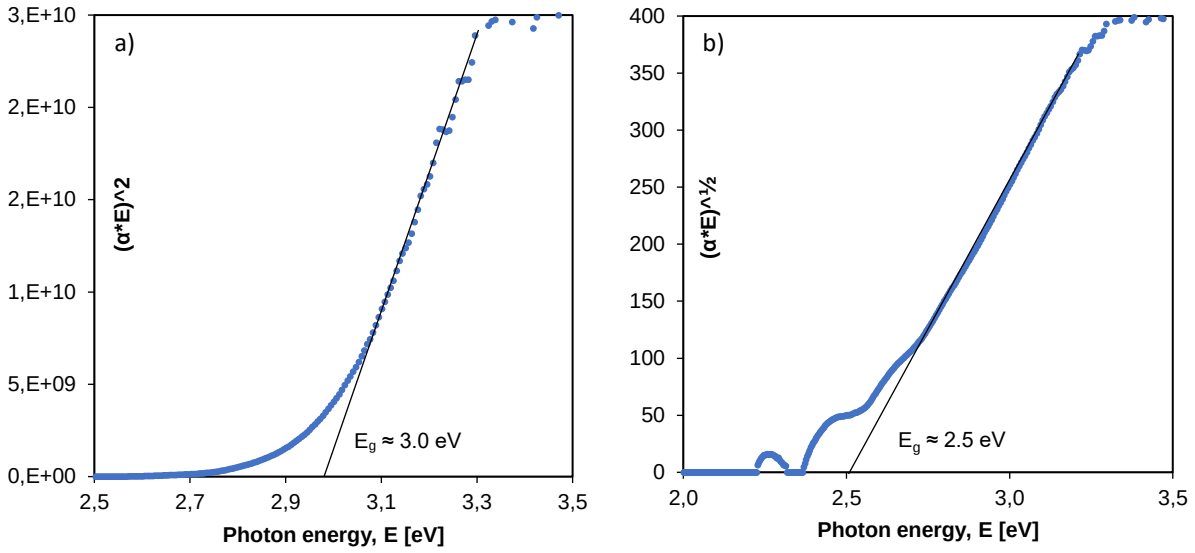

Figure A1.2: Tauc plot for direct *(a)* and indirect *(b)* transitions, calculated from the absorbance data of *Sample 1.0*. The bandgaps, E_g, were estimated by extrapolating the linear regions. A represents the absorption coefficient, which is of the order of magnitude 10^4 cm^{-1}.

A2. Filter properties

Two types of filters were used in this project: neutral density filters (intensity experiments), and cut-on filters (wavelength experiment).

Figure A2.1 shows the ideal and recorded power transmitted by the neutral density filters. The ideal transmission was calculated from the equation given in the plot, based on the transmission recorded without filter. The discrepancy between the ideal and measured transmission cannot be explained by the observed random fluctuations, which were approximately ± 1 mW. *Figure A2.2* illustrates the corresponding transmission spectra of each filter; all are within expected accuracy.

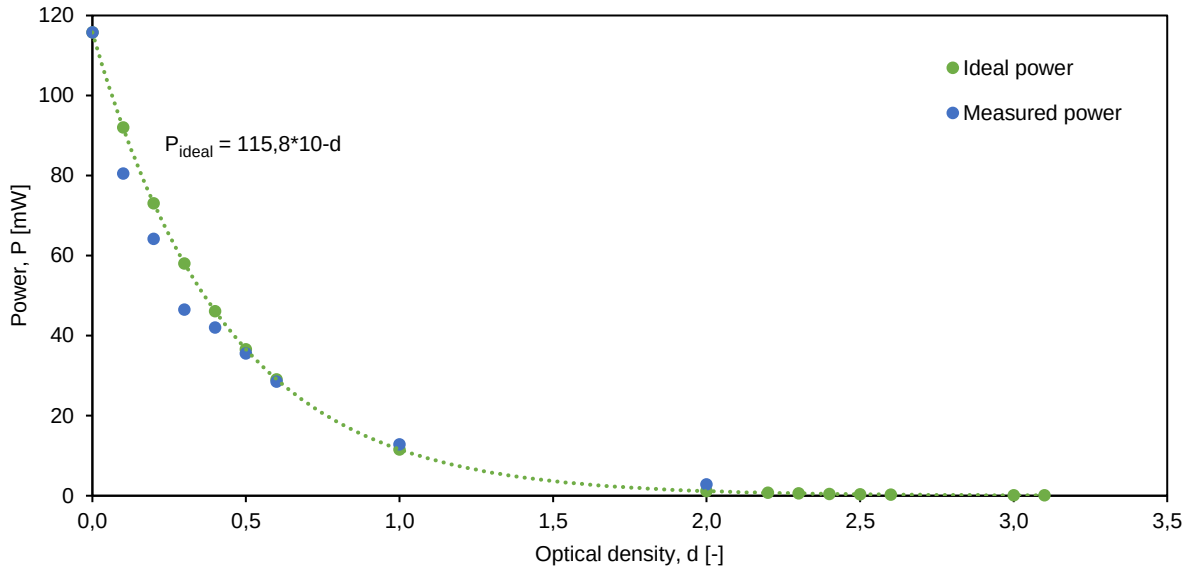

Figure A2.1: The ideal and recorded power transmitted by neutral density filters. An optical density of *d = 0* means that no filter was applied.

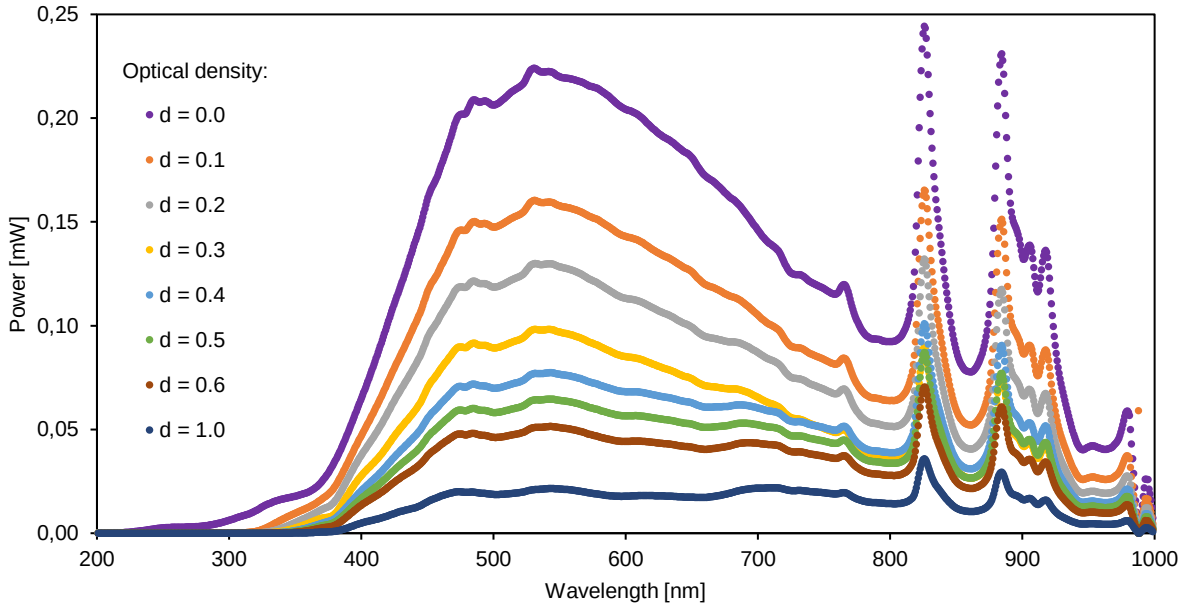

Figure A2.2: Recorded power transmitted by neutral density filters. An optical density of *d = 0* means that no filter was applied.

Figure A2.3 and A2.4 illustrate the total transmitted power and the transmission spectra of the cut-on filters, respectively. Ideally, these filters should only exclude wavelengths below the given cut-on wavelength. However, since the filters are not ideal, they have a significant absorbance in the entire spectrum. As apparent from the spectra, the absorption is typically strongest at shorter wavelengths. Recall that the total power without filter was 116 mW.

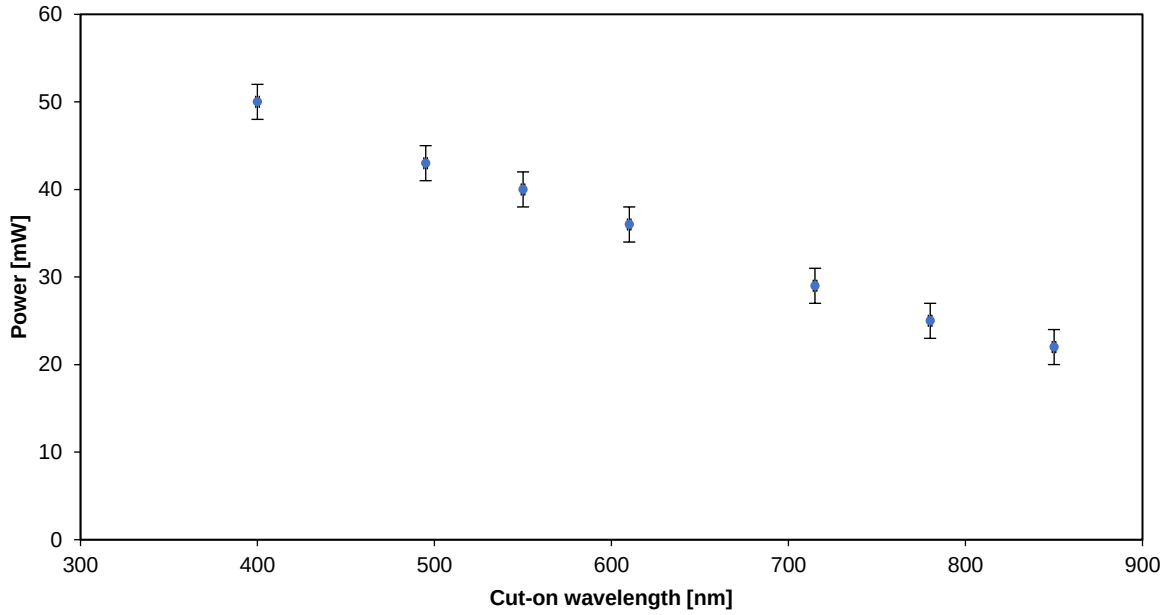

Figure A2.3: Recorded power transmitted by cut-off filters. The error bars illustrate the random fluctuations.

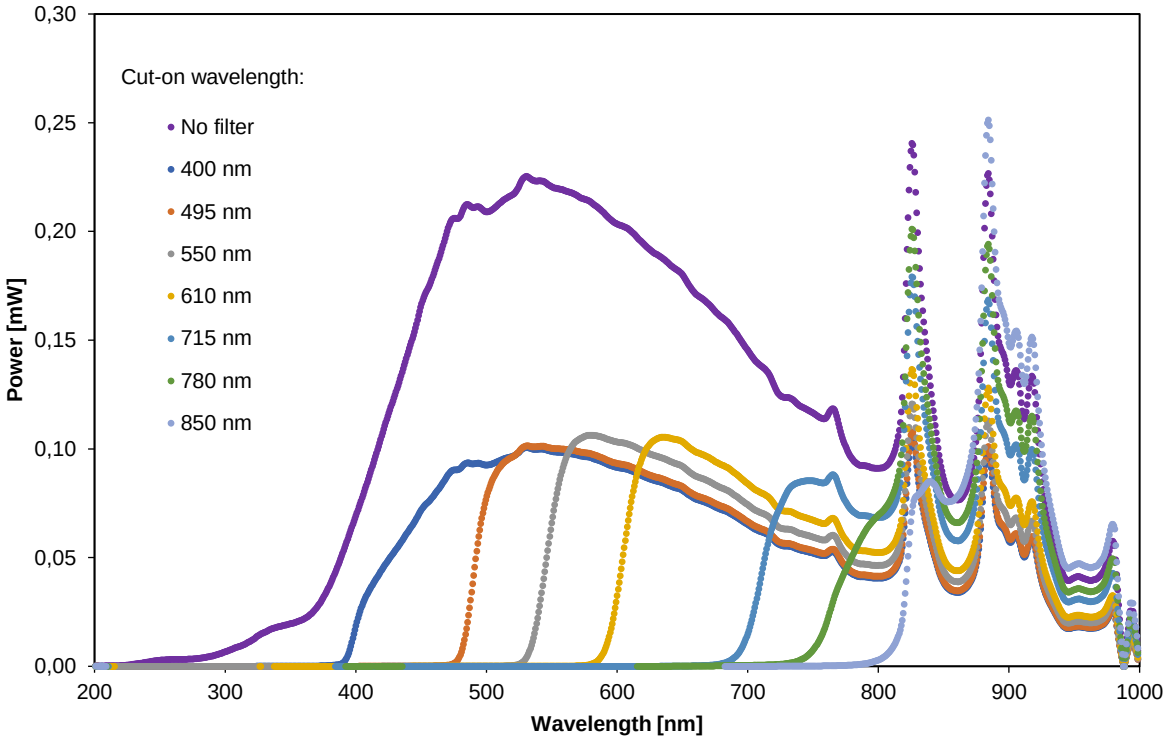

Figure A2.4: Recorded power spectra transmitted by cut-off filters.

A3. The effect of temperature

This section contains additional data from the temperature experiments.

Figure *A3.1* shows the complete datasets of the temperature and transmittance during bleaching, when initiating the heating and bleaching simultaneously. See *Section 4.3.2* for a full discussion.

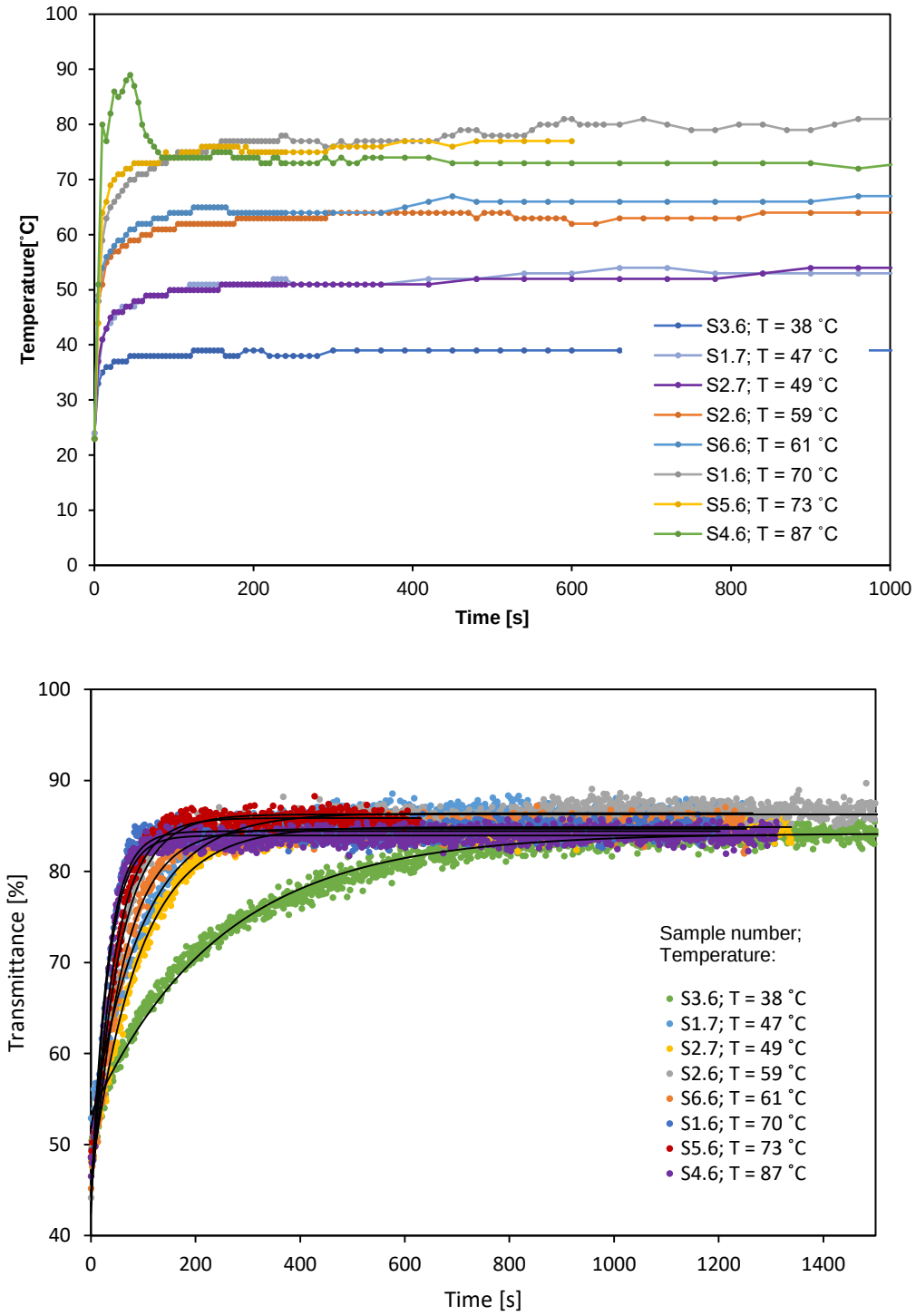

Figure A3.1: Temperature *(a)* and time-resolved transmittance *(b)*: Bleaching while heating the samples.

Figure A3.2 shows the temperature during photodarkening and thermal bleaching, when the samples were preheated. The temperature was kept as constant as possible, and the maximum temperature fluctuation observed was ±2 ˚C. *Figure A3.3* shows the time-resolved transmittance during photodarkening at different temperatures. See *Section 4.3.3* for a full discussion.

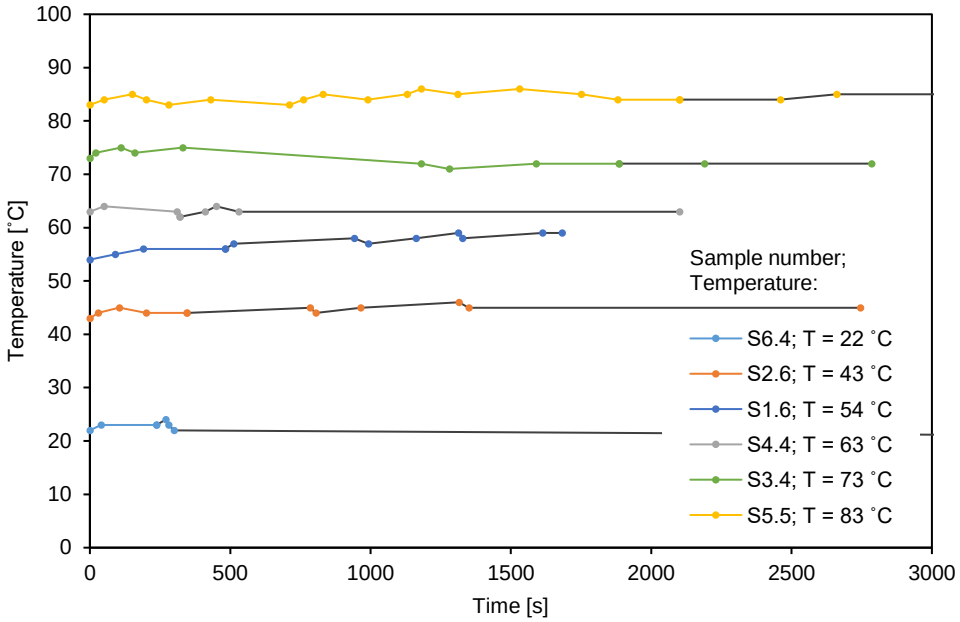

Figure A3.2: Temperature during photodarkening (coloured lines) and thermal bleaching (black lines) during the final temperature experiment. The temperature was monitored continuously, and each temperature increase/decrease is represented by a data point.

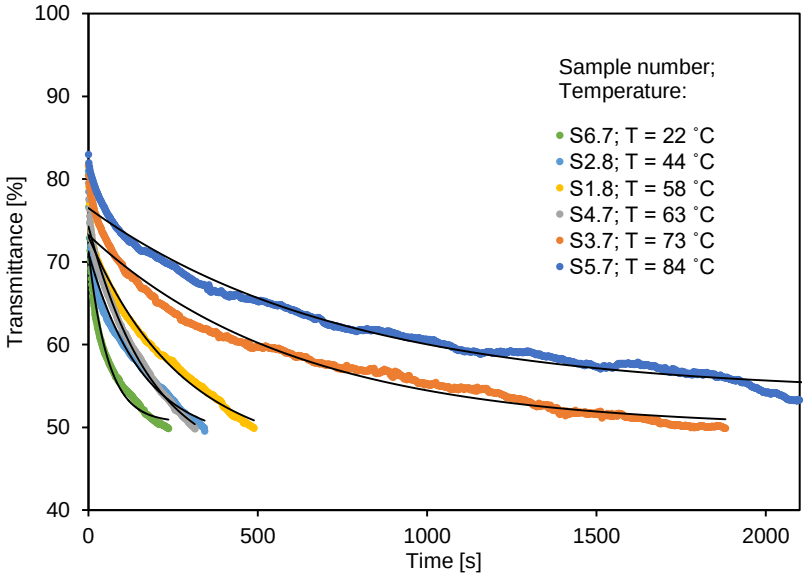

Figure A3.3: Time-resolved transmittance during photodarkening, after pre-heating to a stable temperature. Measured data (coloured) and fitted exponential curves (black).

A4. The effect of incident wavelength

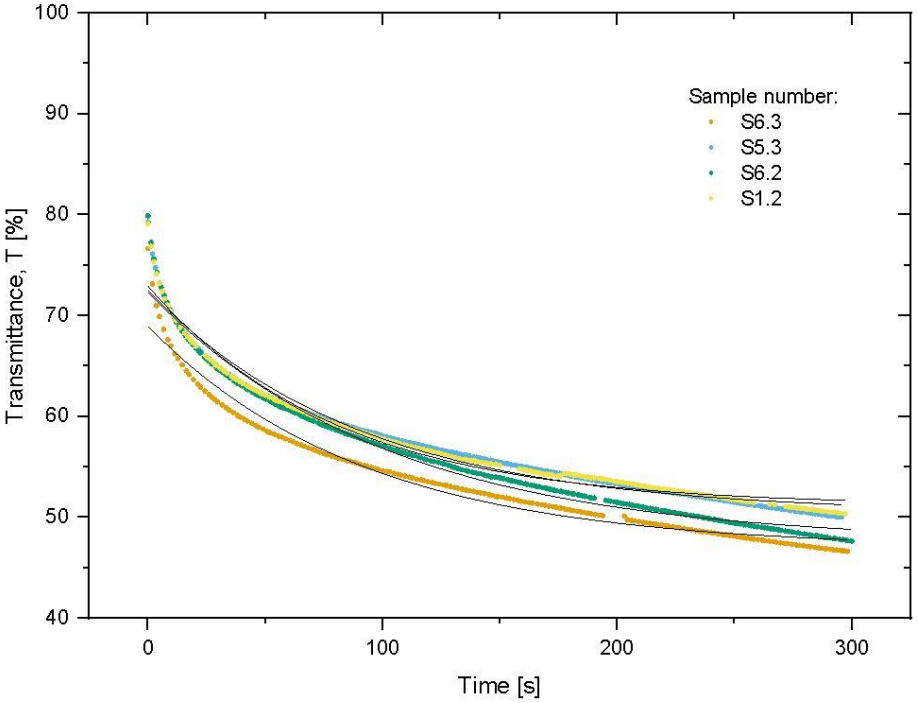

Figure A4.1: Bleaching when illuminated by different wavelengths; Average transmittance in 500-900 nm interval.

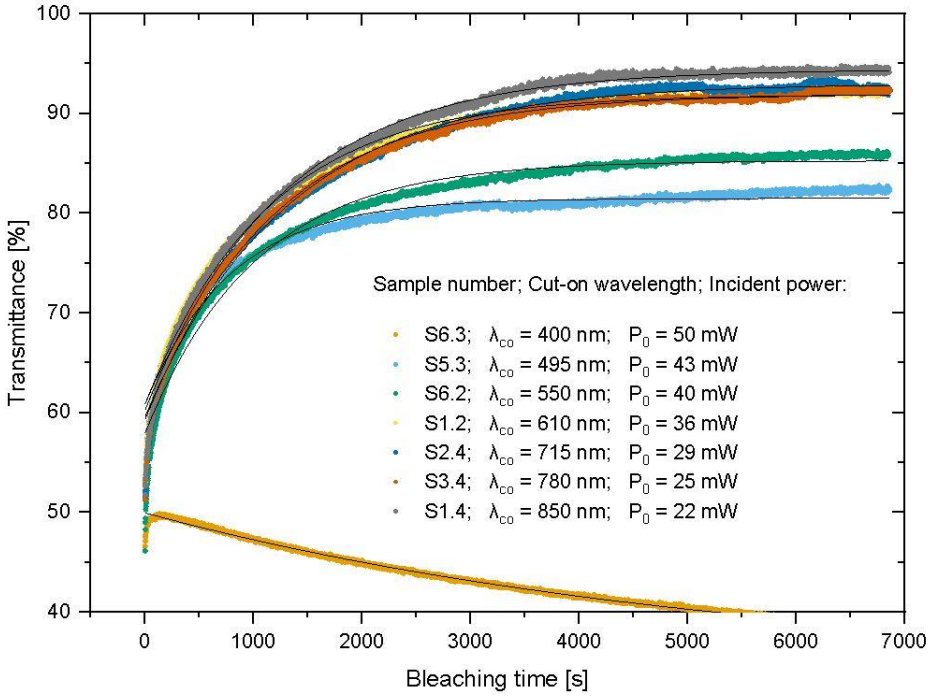

Figure A4.2: Bleaching when illuminated by different wavelengths; Average transmittance in 900-1000 nm interval. When using the filter with a cut-on wavelength of 400 nm, *Sample 6.3* did not regenerate. The trends are similar to those calculated for the 500-900 nm interval (*Section 4.5*)

Norges miljø- og biovitenskapelige universitet
Noregs miljø- og biovitskapelege universitet
Norwegian University of Life Sciences

Postboks 5003
NO-1432 Ås
Norway